HEALTH AND MEDICINE

Targeting TRPC channels for control of arthritis-induced bone erosion

Suravi Ray[1]†, Jamie L. McCall[2,3]†, Jin Bin Tian[4], Jaepyo Jeon[4], Aidan Douglas[1], Kendall Tyler[1], Siyao Liu[5,6], Kendyl Berry[2,3], Brady Nicewarner[3], Casey Hall[3], Klaus Groschner[7], Bernadett Bacsa[7], Werner Geldenhuys[8,9,10], Michael X. Zhu[4], Harry C. Blair[11], John B. Barnett[2,3,10]*, Jonathan Soboloff[1]*

Arthritis leads to bone erosion due to an imbalance between osteoclast and osteoblast function. Our prior investigations revealed that the Ca^{2+}-selective ion channel, Orai1, is critical for osteoclast maturation. Here, we show that the small-molecule ELP-004 preferentially inhibits transient receptor potential canonical (TRPC) channels. While ELP-004 minimally affected physiological RANKL-induced osteoclast maturation in murine bone marrow– and spleen-derived myeloid cells (BMSMCs) and human PBMC-derived cells, it potently interfered with osteoclast maturation driven by TNFα or LTB4. The contribution of TRPC channels to osteoclastogenesis was examined using BMSMCs derived from TRPC4$^{-/-}$ or TRPC(1–7)$^{-/-}$ mice, again revealing preferential interference with osteoclastogenesis driven by proinflammatory cytokines. ELP-004 also reduced bone erosion in a mouse model of rheumatoid arthritis. These investigations reveal TRPC channels as critical mediators of inflammatory bone erosion and provide insight into the major target of ELP-004, a drug currently in preclinical testing as a therapeutic for inflammatory arthritis.

INTRODUCTION

Acute inflammation related to arthritis can occur in solitary sites after trauma or result from infections, such as in lyme disease, in adults or children. In these isolated cases, the cause is often not identified (*1*). In contrast, patients with rheumatoid arthritis (RA) have inflammatory patterns indistinguishable from acute arthritis, but with a chronic relapsing time course ultimately resulting in widespread destruction of many joints usually requiring lifelong therapy. While there are infectious causes and genetic predilections, typically RA also is idiopathic. Current treatments for inflammatory arthritis include anti-metabolites, steroids, and biologics, such as tumor necrosis factor–α (TNFα)–blocking molecules, all of which are highly effective, although their efficacy is tempered by debilitating side effects, particularly over the long term (*2*).

Bone erosion is a progressive feature of RA that is caused by a disbalance between bone-forming osteoblasts and bone-resorbing osteoclasts. Physiological osteoclastogenesis is driven by the interaction between receptor activator of nuclear factor κB (NF-κB) (RANK) and its ligand (RANKL), along with macrophage colony-stimulating factor (mCSF) (*3*). mCSF binding to its receptor, c-Fms, provides the signals required for proliferation and survival of osteoclast precursor cells, whereas binding of RANKL to RANK simulates signals required for osteoclast differentiation, survival, and resorptive activity (*3*, *4*). We have previously shown that store-operated Ca^{2+} entry (SOCE) also contributes to osteoclastogenesis (*5*–*7*). However, during acute arthritis and other inflammatory conditions, increased levels of inflammatory cytokines [particularly TNFα; (*8*)] leads to increased osteoclastogenesis, primarily due to cross talk with RANK-mediated pathways [for example, generation of NF-κB (*9*)]. Moreover, inflammatory RA is known to cause chronic synovial membrane inflammation and bone erosion in joints, which can lead to an increased production of leukotriene B4 (LTB4) (*10*), and the binding of LTB4 to its receptor [leukotriene B4 receptor 1 (BLT1)] can elevate intracellular Ca^{2+} concentration and accelerate TNFα release from neutrophils (*10*). Reciprocally, TNFα induces LTB4 production via activation of phospholipase A2 (PLA2) (*11*, *12*), 5-lipoxygenase (5-LOX) (*13*), and leukotriene A4 (LTA4) hydrolase, which drive arachidonic acid release and subsequent conversions to LTA4 (*13*) and LTB4, respectively. Therefore, while TNFα is a clinically effective therapeutic target for the treatment of arthritis, LTB4 is also a potent proinflammatory cytokine that is upregulated in RA patients with active arthritis (*14*) working in concert with TNFα in this disease. Hence, the current investigation focuses on both molecules.

The differentiation of osteoclasts from monocytes and their attachment to bone for resorption depend on inositol (1,4,5) trisphosphate ($InsP_3$)–mediated Ca^{2+} release from the endoplasmic reticulum (ER) (*15*). The resultant ER Ca^{2+} depletion leads to the activation of stromal interacting molecule (STIM) proteins, which activate Orai channels, a process known as SOCE (*5*). In addition, members of the transient receptor potential canonical (TRPC) nonselective cation channel family are simultaneously activated by overlapping signals (*16*). These lead to increased cytosolic Ca^{2+} levels that activate

[1]Fels Cancer Institute for Personalized Medicine, Department of Cancer & Cellular Biology, Lewis Katz School of Medicine at Temple University, Philadelphia, PA 19140, USA. [2]Department of Microbiology, Immunology & Cell Biology, West Virginia University School of Medicine, Morgantown, WV 26506, USA. [3]*ExesaLibero* Pharma, Morgantown, WV 26505, USA. [4]Department of Integrative Biology and Pharmacology, McGovern Medical School, The University of Texas Health Science Center at Houston, Houston TX 77030, USA. [5]Center for Translational Cancer Research, Institute of Biosciences and Technology, Texas A&M University, Houston, TX 77030, USA. [6]Department of Translational Medical Sciences, School of Medicine, Texas A&M University, Houston, TX 77030, USA. [7]Medical University of Graz, Division of Medical Physics and Biophysics, Neue Stiftingtalstrasse 6/H03, 8010 Graz, Austria. [8]Department of Pharmaceutical Sciences, West Virginia University School of Pharmacy, Morgantown, WV 26506, USA. [9]Department of Neuroscience, West Virginia University School of Medicine, Morgantown, WV 26506, USA. [10]West Virginia University Cancer Institute, Morgantown, WV 26506, USA. [11]Research Service, VA Medical Centre, Departments of Pathology and of Cell Biology, University of Pittsburgh, Pittsburgh, PA, 15261, USA.
*Corresponding author. Email: soboloff@temple.edu (J.S.); johnb@exesaliberopharma.com (J.B.B.)
†These authors contributed equally to this work.

calcineurin (*17*), ultimately driving the nuclear translocation of the transcription factor Nuclear Factor of Activated T Cells 1 (NFATc1), which promotes the expression of a number or genes required for osteoclastogenesis (*18*).

The current investigation focuses primarily on TRPC channels. Although TRPCs have been extensively investigated as potential store-operated Ca^{2+} channels (*19*–*21*), they are primarily activated by receptors that signal through phospholipase C (PLC). PLCs are widely expressed enzymes typically activated by a large range of G protein–coupled receptors (GPCRs) and receptor tyrosine kinases (RTKs). In particular, PLCβ isoforms are activated through GPCR coupling to G_q family of heterotrimeric G proteins (*22*). Upon activation, PLC hydrolyses phosphatidylinositol 4,5-bisphosphate (PIP_2) into diacylglycerol (DAG) and $InsP_3$. Both the loss of PIP_2 and production of DAG have been shown to contribute to activation of TRPC channels (*23*). Furthermore, the activation of TRPC4 and TRPC5 can be strongly potentiated by $G_{i/o}$ proteins (*24*). Although prior investigations have suggested that TRPC channels promote osteoclastogenesis (*25*, *26*), the therapeutic potential of these findings have not been explored, and the roles of TRPCs in osteoclast function remain poorly defined.

Our previous investigations supported a role for SOCE in osteoclastogenesis (*5*). Hence, suppressing SOCE via small interfering RNA targeting Orai1 (the pore-forming unit of the store-operated Ca^{2+} channel) or the antagonist, 3,4-dichloropropionanilide reduced the formation of bone-degrading osteoclasts in vitro (*5*). Further, both global Orai1 knockout and conditional Orai1 deletion in myeloid cells interfered with osteoclast multinucleation in mice (*6*, *7*), and the remaining mononuclear cells retained a limited ability to degrade bone (*27*), which was sufficient to avoid osteopetrosis. Given the critical role of osteoclasts in bone erosion within the context of arthritis, these investigations led us to assess the possibility that 3,4-dichloropropionanilide and/or 3,4-dichloropropionanilide analogs might provide safe protection from arthritic bone erosion (*27*). However, neither 3,4-dichloropropionanilide nor its analogs blocked RANKL-induced osteoclast differentiation in vitro at concentrations below 10 μM (*5*), yet we now find that serum levels of these agents are orders of magnitude lower in vivo. Therefore, we reasoned that these drugs might have a different target other than Orai1, especially within the context of arthritis. ELP-004 is a methylated 3,4-dichloropropionanilide analog designed to preclude metabolizing to 3,4-dichloroaniline and propionic acid (*28*), erythrotoxic metabolites associated with increased methemoglobin, enhanced erythropoiesis, and persistent hemosiderosis. Our preclinical testing in mice has demonstrated that ELP-004 shows promising pharmacokinetic and metabolism profiles without inducing genotoxic or extensive off-target toxicities (*29*). Hence, the current investigation focuses on identifying the new ELP-004 target(s) and defining the distinct contexts that would cause arthritis-induced bone erosion to be facilitated by a different gene than physiological bone maintenance. Here, we find that TRPC channels serve a mediatory role in both LTB4- and TNFα-induced osteoclastogenesis, representing a bona fide target for therapeutic intervention.

RESULTS

ELP-004 inhibits TRPC channels with a high potency

We have previously reported that 3,4-dichloropropionanilide inhibits Orai channels (*5*, *27*). To assess the STIM/Orai subtype specificity of ELP-004, HEK293 cells stably overexpressing all STIM/Orai combinations (STIM1/Orai1, STIM1/Orai2, STIM1/Orai3, STIM2/Orai1, STIM2/Orai2, and STIM2/Orai3) were used. To induce SOCE, cells plated on coverslips were loaded with Fura2 and then treated with varying concentrations (0 to 1 mM) of ELP-004 along with Thapsigargin (Tg; 2 μM; 10 min), an inhibitor of the sarco/endoplasmic reticulum calcium ATPase (SERCA) pump, to deplete ER Ca^{2+} content in a nominally Ca^{2+}-free extracellular solution. SOCE was induced with 1 mM extracellular Ca^{2+}. To assess the ability of ELP-004 to inhibit SOCE, the magnitude of cytosolic Ca^{2+} elevation was measured in each cell line, followed by nonlinear dose response regression analysis (fig. S1). STIM2-overexpressing cell lines exhibited a several fold lower median inhibitory concentration (IC_{50}) than STIM1-overexpressing cell lines, irrespective of which Orai channel was coexpressed. Given these observations, it seems likely that ELP-004 primarily targets STIM rather than Orai, with STIM2 exhibiting greater ELP-004 sensitivity than STIM1. Further, while ELP-004–mediated STIM1/2 inhibition was very similar in the presence of Orai2 and Orai3 (fig. S1, B and C, respectively), ELP-004–mediated Orai1 inhibition was amplified in the presence of STIM2, while STIM1/Orai1-mediated Ca^{2+} entry was largely unaffected by ELP-004 (fig. S1A). While we were intrigued by these observations, the lowest ELP-004 IC_{50} observed for any combination of STIM and Orai was still a relatively high 10 μM (STIM2/Orai1; fig. S1A). Given prior evidence of pharmacological overlap between SOCE- and TRPC-mediated Ca^{2+} entry (*19*) along with their shared roles in PLC-mediated Ca^{2+} entry, we focused primarily on the possibility that ELP-004 may inhibit TRPC-mediated Ca^{2+} entry.

To measure ELP-004–dependent inhibition of TRPC-mediated Ca^{2+} entry, we tested human embryonic kidney (HEK) 293 cells stably expressing TRPC3 or TRPC6. Alternatively, TRPC4–green fluorescent protein (GFP), TRPC5-GFP, and TRPC7-GFP were introduced by transient transfection into HEK293 cells via electroporation to assess Ca^{2+} entry. Because TRPC3, TRPC6, and TRPC7 can be directly activated by DAG (*19*), TRPC3/6/7-expressing cells were treated with ELP-004 (0 to 1 mM) for 10 min before challenging with 1-Oleoyl-2-acetyl-*sn*-glycerol (OAG), a membrane permeable form of DAG (Fig. 1, A to C). OAG stimulated rapid Ca^{2+} entry in untreated TRPC-expressing cells, which was inhibited by ELP-004 with an IC_{50} of 1 to 2 μM (Fig. 1D), representing a two order of magnitude increase in efficacy relative to endogenous SOCE (IC_{50} = 100 μM). However, the elevation of Ca^{2+} content and an altered time course of OAG-induced activation were noted in TRPC3-overexpressing cells. Distinct from other TRPC channels, TRPC3 exhibits low-level constitutive activity, which may complicate interpretation.

Unlike TRPC3/6/7, TRPC4 and TRPC5 are not activated by DAG alone (*30*). Therefore, to determine whether ELP-004 inhibits TRPC4 or TRPC5, we assessed its ability to inhibit carbachol (Cch)–induced Sr^{2+} entry. As previously reported, Sr^{2+} passes through nonselective TRPC channels, but not the highly Ca^{2+}-selective Orai channels (*19*, *30*); the impermeability of $HEK293_{WT}$ cells to Sr^{2+} after either store depletion or Cch addition (fig. S2A) was confirmed. However, with TRPC4, TRPC5, or TRPC7 overexpressed, potent Cch-induced Sr^{2+} entry was observed (Fig. 1, E to H). While ELP-004 (1 nM to 100 μM) had no effect on Cch-induced ER Ca^{2+} release (Fig. 1, E to G), it suppressed the increase in Fura2 ratios caused by subsequent additions of Sr^{2+} (3 mM) in both TRPC4- and TRPC5-expressing cells by 1 to 2 orders of magnitude (IC_{50} = 11.5 nM for TRPC5 and 172.4 nM for TRPC4; Fig. 1H) higher efficiency than observed for TRPC3/6/7 (Fig. 1D). Last, to assess any possible

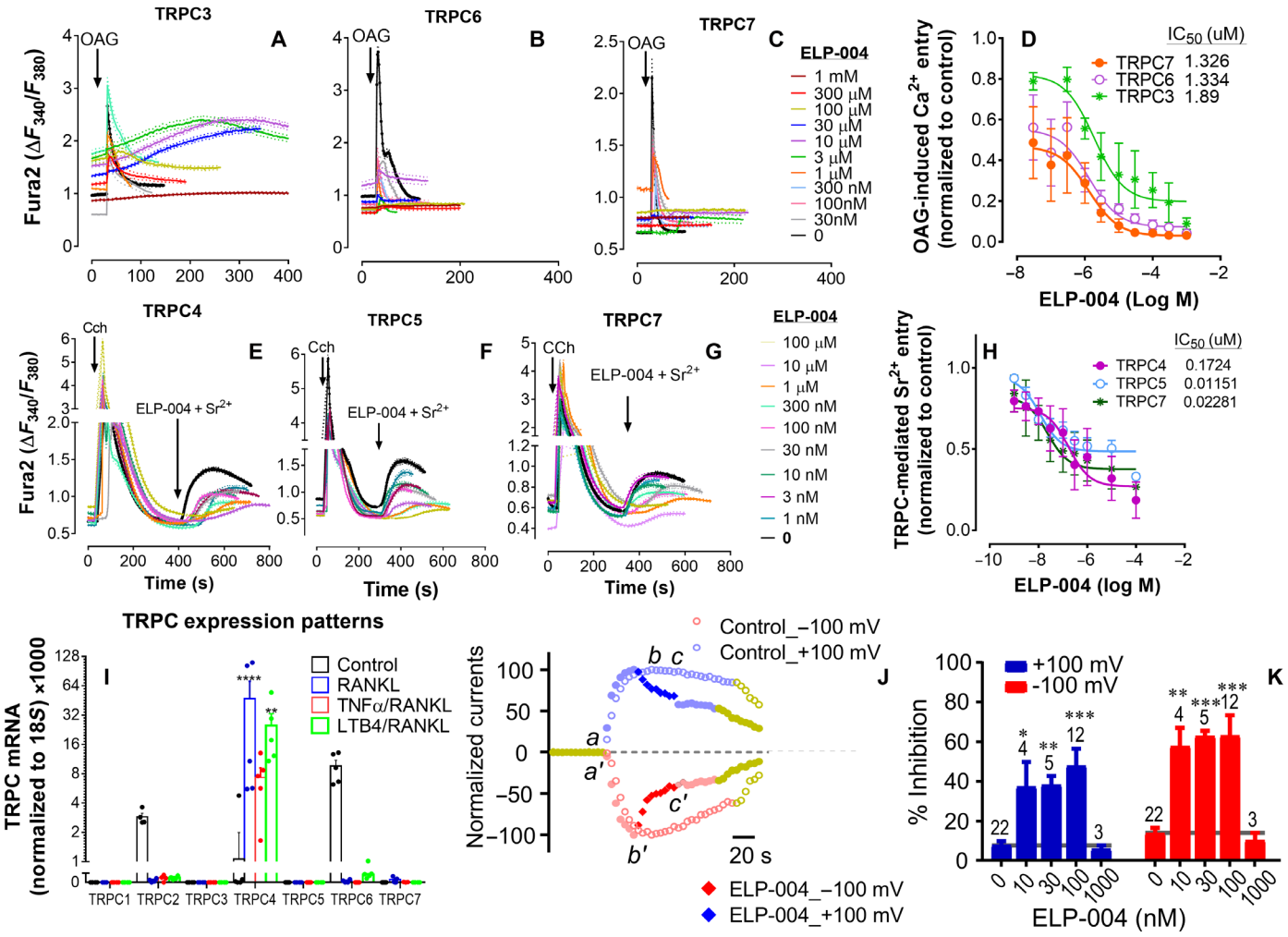

Fig. 1. ELP-004 is a TRPC inhibitor. (**A** to **D**) TRPC3-, TRPC6-, and TRPC7-overexpressing HEK293 cells ($n = 3$ to 5) plated on coverslips were loaded with Fura2-acetoxymethyl ester (Fura2-AM) (2 μM) before treating with 100 μM OAG (1-oleoyl-2-acetyl-*sn*-glycerol), Ca^{2+} (1 mM), and ELP-004 (0-1 mM). Each representative trace represents 50 to 100 cells with SEM shown as a dotted line. (D) Ca^{2+} entry was measured, normalized to control and then plotted to calculate IC_{50}s by nonlinear regression. (**E** to **H**) TRPC4-, TRPC5-, and TRPC7-overexpressing HEK293 cells ($n = 3$ to 5) plated on coverslips were loaded with Fura2-AM (2 μM) before treating with Cch (100 nM), Sr^{2+} (3 mM), and ELP-004 (0 to 100 μM). (H) Sr^{2+} entry was measured, normalized to control and then plotted to calculate IC_{50}s by nonlinear regression. (**I**) qPCR for TRPC(1–7) and 18*S* RNA was performed in murine BMSMCs incubated for 14 days under the indicated conditions ($n = 3$). Data were analyzed by two-way ANOVA with Dunnett's multiple comparisons [*P*(TRPC expression) < 0.0001, *P*(treatment) = 0.2479, *P*(interaction) = 0.0029]. Data below log2(x) = 1 not shown. (**J**) Representative traces of whole-cell currents at ±100 mV for HEK293 cells transiently expressing mouse TRPC4β. Cells in nominally Ca^{2+}-free bath solution (30 s) were treated with 30 nM Englerin A (EA). At ~10 s after the +100 mV current peak, EA (control), or EA plus ELP-004 (ELP-004, 30 nM) was applied; yellow-green points indicate washout. Currents were normalized to that at the peak. *a*, *b*, *c*, *a′*, *b′*, and *c′* indicate the time points where current-voltage curves are displayed in fig. S2. (**K**) Summary of current decrease 45 s after the peak ±10, 30, 100, and 1000 nM ELP-004. Data are presented as means ± SEM. Cell numbers (*n*) are labeled above each column. Significant differences compared to the desensitization (0) group were assessed with one-way ANOVA followed by Dunnett's multiple comparisons. **P* < 0.05, ***P* < 0.01, and ****P* < 0.001

differences in ELP-004–mediated TRPC inhibition associated with the different assays used, ELP-004 inhibition of TRPC7-mediated Sr^{2+} entry following Cch stimulation was also measured (Fig. 1, G and H). An order of magnitude increase in sensitivity was again observed using this assay (IC_{50} = 22.8 nM versus 1.33 μM), suggesting that receptor-mediated TRPC activation is more sensitive to ELP-004 than direct DAG-mediated TRPC activation.

Given the limited information available on TRPC channel expression and their role in osteoclast differentiation and maturation, we measured TRPC expression during osteoclastogenesis by quantitative polymerase chain reaction (qPCR) (Fig. 1I). Murine bone marrow– and spleen-derived myeloid cells (BMSMCs) were incubated for 14 days under several different conditions. All conditions included mCSF (50 ng/ml), which is necessary to support growth and survival; cells treated in mCSF only form macrophages, while mCSF plus RANKL (100 ng/ml) is a standard osteoclastogenesis protocol (*5*). In addition, because 100 nM 3,4-dichloropropionanilide failed to inhibit RANKL-induced osteoclastogenesis (*5*), we considered the possibility that arthritis-induced osteoclastogenesis might depend on the presence of proinflammatory factors with differential dependence on TRPC channels. TNFα has been shown

to promote osteoclastogenesis in a prior study in the presence of low-dose RANKL (1 ng/ml as opposed to 100 ng/ml) (*31*). While TNFα would not be predicted to activate a TRPC channel, LTB4 would. As discussed in the Introduction, TNFα and LTB4 stimulate each other's expression in a positive feedback loop (*10*–*14*). Further, TNFα is a clinically relevant target in arthritis (*32*). Hence, over the course of this study, we have also examined both TNFα (2 ng/ml)– and LTB4 (50 nM)–induced osteoclastogenesis, all in the presence of mCSF (50 ng/ml) and RANKL (1 ng/ml). No significant expression of TRPC1, TRPC3, TRPC5, or TRPC7 could be detected under any conditions. Macrophages (control) expressed relatively high levels of both TRPC2 and TRPC6 and modest but detectable TRPC4 (Fig. 1I). However, all conditions supporting osteoclast differentiation demonstrated at least a 50-fold increase in TRPC4 expression compared to macrophages (Fig. 1I). While we fully recognize that mRNA and protein levels are not necessarily the same, these observations led us to assess the possibility that TRPC4 is the primary TRPC subtype expressed in murine osteoclasts, while macrophages may primarily use TRPC2 and TRPC6. Considered alongside the fact that all TRPCs exhibited relatively high sensitivity to ELP-004, we assessed the possibility that ELP-004 inhibits osteoclastogenesis in arthritis through TRPC4.

Because TRPC4 was the primary TRPC channel expressed in osteoclasts, we used whole-cell patch clamp recording to determine whether ELP-004 inhibits TRPC4-mediated currents. TRPC4-overexpressing HEK293 cells were first stimulated with a highly selective TRPC4/5 activator Englerin A (EA; 30 nM) (*33*) in a nominally Ca^{2+}-free bath solution, which induced robust monovalent cation currents at both positive and negative potentials (Fig. 1J). After the currents reached the peak, ELP-004 (10 to 1000 nM) was applied to see if it affected the current decline. In the absence of ELP-004, the EA-induced TRPC4 currents decreased by ~8 and ~14% at +100 and −100 mV, respectively, 45 s after the peak, representing moderate desensitization (Fig. 1, J and K). In the presence of as low as 10 nM ELP-004, the decreases reached 37 and 58% at +100 and −100 mV, respectively, indicative of an instant inhibition by the drug. Higher ELP-004 concentrations (30 and 100 nM) did not show stronger inhibitory effects, and at 1 μM, ELP-004 lost its inhibitory action on the EA-induced currents (Fig. 1K). Plausibly, ELP-004 is an allosteric modulator with both inhibitory and facilitatory (at higher concentrations) effects on the TRPC4 channel, at least with respect to monovalent cation currents activated by EA. This may be somewhat different from Sr^{2+} entry induced through receptor-mediated signaling, which showed persistent inhibition at 1 μM and above (Fig. 1E). Nonetheless, the rapid action of nanomolar ELP-004 on the EA-evoked TRPC4 currents suggests that it is a potent fast acting inhibitor on the TRPC4 channel. Because this observation may reflect a complex mechanism of ELP-004 actions on TRPC channels sensitive to the concentrations used, all subsequent experiments were performed using 100 nM ELP-004, a concentration also well below the sensitivity of Orai channels.

ELP-004 inhibits basal Ca^{2+} and related NFATc1 translocation in inflammatory cytokine-dependent osteoclastogenesis

Ca^{2+} is a critical mediator of osteoclastogenesis both due to its essential role in NFAT activation (*34*, *35*) and its contribution to multinucleation (*5*–*7*). Therefore, we performed a series of experiments assessing how ELP-004 (100 nM) affects osteoclastogenesis. At this concentration, ELP-004 inhibits TRPC channels (Fig. 1) without affecting Orai (fig. S1). Consistent with previous findings (*5*), osteoclastogenesis was accompanied by increased basal intracellular Ca^{2+} level by day 7, which was sustained through day 21 (Fig. 2, A and B, and fig. S3, A to C), irrespective of whether or not differentiation was induced by RANKL alone (Fig. 2A and fig. S3A) or together with either TNFα (Fig. 2B and fig. S3B) or LTB4 (figs. S3C and S4A). Notably, ELP-004 (100 nM) had no significant effect on Ca^{2+} levels during RANKL-induced osteoclastogenesis (Fig. 2A and fig. S3A) but significantly attenuated Ca^{2+} elevation driven by TNFα (Fig. 2B and fig. S3B) or LTB4 (figs. S4A and S3C). Next, we examined NFATc1 translocation at the same time points as for basal intracellular Ca^{2+} levels. Similar to changes in basal Ca^{2+}, significant

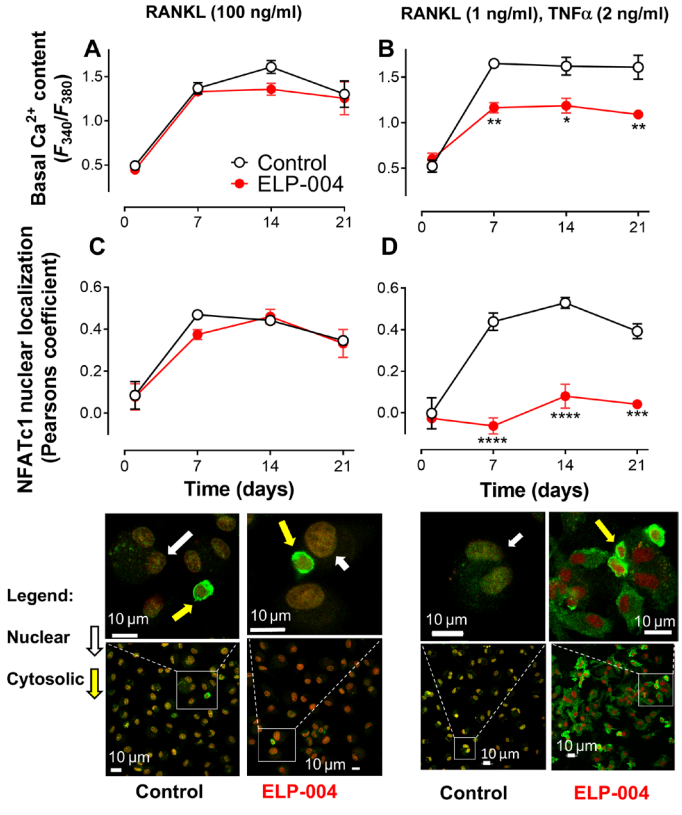

Fig. 2. ELP-004 inhibits basal calcium and related NFATc1 translocation in inflammatory cytokine-dependent osteoclastogenesis. Murine BMSMCs were differentiated to form osteoclasts using mCSF (50 ng/ml) and RANKL (100 ng/ml) (**A** and **C**) or mCSF (50 ng/ml), RANKL (1 ng/ml), and TNFα (2 ng/ml) (**B** and **D**). (A and B) Cells plated on coverslips were loaded with Fura2-AM (2 μM) and treated as indicated in the presence or absence of ELP-004 (100 nM) before measuring basal Ca^{2+} concentration at days 1,7,14, and 21. ELP-004 had no effect on basal Ca^{2+} levels during RANKL-induced osteoclastogenesis (two-way ANOVA, $P > 0.05$), but significantly inhibited basal Ca^{2+} for TNFα-induced [TNFα: two-way ANOVA, P(ELP-004) < 0.0001, P(time) < 0.0001, P(interaction) = 0.0260]. (C and D) At the same time points, NFATc1 nuclear translocation was measured by immunocytochemistry; 7-aminoactinomycin D (7-AAD) was used to stain the nucleus. Average Pearson's correlation of NFATc1 colocalization with nuclear signal was calculated for 50 to 100 cells; representative images of each condition are displayed below. ELP-004 had no significant effect on NFATc1 colocalization in RANKL-induced osteoclasts as determined by two-way ANOVA, although increased nuclear translocation was observed throughout the incubation [P(time) < 0.0001; (C)]. ELP-004 significantly inhibited NFATc1 colocalization for TNFα-induced osteoclasts [two-way ANOVA P(ELP-004) < 0.0001, P(time) < 0.0001, P(interaction) = 0.0002; (D)]. *P < 0.05, **P < 0.01, ***P < 0.001, and ****P < 0.0001.

NFAT nuclear localization was observed in response to RANKL (Fig. 2C) or together with TNFα (Fig. 2D) or LTB4 (fig. S4B) by day 7, which was sustained through day 21. While ELP-004 had no effect on RANKL-induced NFAT translocation (Fig. 2C), it blocked NFAT nuclear localization in response to TNFα (Fig. 2D) or LTB4 (fig. S4B). No significant changes in NFAT localization were observed after ELP-004 treatment in response to the low concentration of RANKL alone (1 ng/ml; fig. S5A) or in BMSMC-derived macrophages (fig. S6A). Considered collectively, these observations suggest a critical role for TRPC channels in NFAT nuclear localization in inflammatory cytokine-induced osteoclastogenesis, distinct from physiological RANKL-induced osteoclastogenesis, which is insensitive to ELP-004 and likely dependent on Orai function, consistent with prior study (*36*). These data reveal a previously unknown role for TRPC channels in osteoclastogenesis associated with inflammatory conditions.

ELP-004 is more effective at inhibiting inflammatory osteoclastogenesis than physiological osteoclastogenesis

To determine whether inhibition of osteoclastogenesis by ELP-004 is dependent on the presence of inflammatory cytokines, we compared multiple parameters of osteoclastogenesis in murine BMSMCs cultured in the presence of RANKL (Fig. 3), TNFα/RANKL (Fig. 4), or LTB4/RANKL (fig. S7). At each time point (days 1 to 21), cells were fixed and stained for tartrate-resistant acid phosphatase (TRAP) activity, which is an essential component produced by osteoclasts during bone resorption. Minimal TRAP-positive cells were detected in negative controls [mCSF (50 ng/ml; fig. S6B), and the addition of RANKL (1 ng/ml) moderately increased the number of TRAP-positive cells (fig. S5B); ELP-004 had no effect under either of these conditions. ELP-004 also had no impact on either the number of TRAP-positive cells or TRAP intensity for osteoclasts differentiated in the presence of RANKL (100 ng/ml) (Fig. 3A). The number of TRAP-positive cells approached 100% by day 14, yet TRAP signal intensity continued to increase after day 14 (Fig. 3A). Next, we assessed the effect of ELP-004 on RANKL-induced multinucleation. The number of multinuclear cells increased throughout the course of this 21-day experiment [two-way analysis of variance (ANOVA), $P = 0.0001$], which was inhibited overall by ELP-004 ($P < 0.01$; Fig. 3B), although no significant differences at any specific time point could be detected. To assess control of osteoclast function, cells were plated on bone biomimetic osteo-assay surface plates and differentiated into osteoclasts as previously described (*5*, *27*). Matrix degradation (or pit formation) was measured after 7, 14, and 21 days; RANKL-induced pit formation gradually increased over time with significant ELP-004–induced inhibition observed on day 21 (Fig. 3C).

The osteoclast fusion proteins DC-STAMP and OC-STAMP serve critical roles in the fusion of osteoclast precursor cells during osteoclastogenesis (*37*); thus, we tested the mRNA expression of both DC-STAMP and OC-STAMP via qPCR (Fig. 3D). Similar to previous studies (*37*, *38*), in the presence of RANKL, Dendritic cell-specific transmembrane protein (DC-STAMP) expression increased over time (two-way ANOVA, $P < 0.01$) in an ELP-004–dependent manner ($P < 0.02$). Significant inhibition was observed at day 14 after ELP-004 treatment (Fig. 3D). Osteoclast stimulatory transmembrane protein (OC-STAMP) expression was an order of magnitude lower throughout the experiment; while there was a trend toward increased expression over time, no significant changes in OC-STAMP expression were observed under these conditions (two-way ANOVA, $P > 0.05$). Further qPCR analysis revealed that ELP-004 inhibited the expression of MMP9, but not other markers of osteoclastogenesis, Vacuolar-type ATPase (V-ATPase) A3, V-ATPASE D2, and Calcitonin receptor (CALCR) at day 14 (fig. S8A). Considered collectively, these data indicate that ELP-004 modestly inhibits some features of RANKL-induced osteoclastogenesis, while many others are ELP-004 resistant.

Next, we assessed whether ELP-004 had any effect on osteoclastogenesis driven by TNFα. Consistent with the prior study, TNFα-induced osteoclastogenesis was induced in the presence of RANKL (1 ng/ml) (*31*). Under these conditions, the number of TRAP-positive cells increased rapidly among days 1, 7, and 14 (reaching ~80%) with nearly all cells being TRAP positive by day 21 (Fig. 4A). TRAP intensity increased continuously between days 1 and 21 (Fig. 4A). ELP-004 treatment had no significant effect on the number of TRAP-positive cells, although TRAP intensity increases were severely attenuated (Fig. 4A). We then counted the number of multinuclear cells, observing a significant increase over time (two-way ANOVA, $P = 0.01$) that was significantly attenuated by ELP-004 ($P < 0.0005$) in a time-dependent manner (interaction $P < 0.05$; Fig. 4B), revealing a generally enhanced effect in the presence of TNFα relative to RANKL alone. Further, the ability of osteoclasts to degrade matrix over time was increased considerably by the presence of TNFα yet completely abolished by ELP-004 (Fig. 4C). These observations reveal that TNFα not only promotes osteoclastogenesis relative to RANKL alone but also does so in a manner highly sensitive to ELP-004.

The mRNA expression of both DC-STAMP and OC-STAMP was ~10-fold lower in the TNFα/RANKL-induced osteoclasts (Fig. 4D) compared to RANKL-induced osteoclasts (Fig. 3D). Irrespective, ELP-004 treatment abrogated the expression of both DC-STAMP and OC-STAMP under these conditions (Fig. 4D). Notably, similar to RANKL-induced osteoclasts, ELP-004 also suppressed MMP9 expression, but no other osteoclast markers (fig. S8B). It is, perhaps, expected that DC-STAMP and OC-STAMP expression would be targetable by ELP-004 because their expression is known to be dependent on Ca^{2+} entry and subsequent NFATc1 activation (*39*). However, it is notable that the 10-fold decrease in expression in RANKL (1 ng/ml)/TNFα (2 ng/ml) relative to RANKL (100 ng/ml) alone was not observed for any other markers. A potential explanation for this would be that TRPC channels contribute to TNFα-induced osteoclast fusion in a manner less dependent on DC-STAMP and OC-STAMP than physiological osteoclastogenesis, although identification of this mechanism will be the subject of a future study.

Last, we assessed whether LTB4 can stimulate osteoclastogenesis (not previously tested) and determined its sensitivity to ELP-004. LTB4 caused an increase in the number of TRAP-positive cells between days 1 and 21 (fig. S7A) in a manner similar to that observed in the presence of RANKL alone (Fig. 3A) or driven by TNFα (Fig. 4A). In addition, similar to the response to TNFα, TRAP intensity increased between days 1 and 21, although it occurred somewhat slowly over the first 14 days (fig. S7A). ELP-004 had no effect on the number of TRAP-positive cells, although it completely prevented the increase in TRAP intensity (fig. S7A). The number of multinuclear cells increased over the first 14 days of this experiment with some loss observed at day 21, potentially reflecting a relatively shorter life span for LTB4-induced osteoclasts (two-way ANOVA, $P = 0.0015$). The presence of ELP-004 led to an overall reduction in osteoclastogenesis ($P = 0.0002$; fig. S7B) with significant

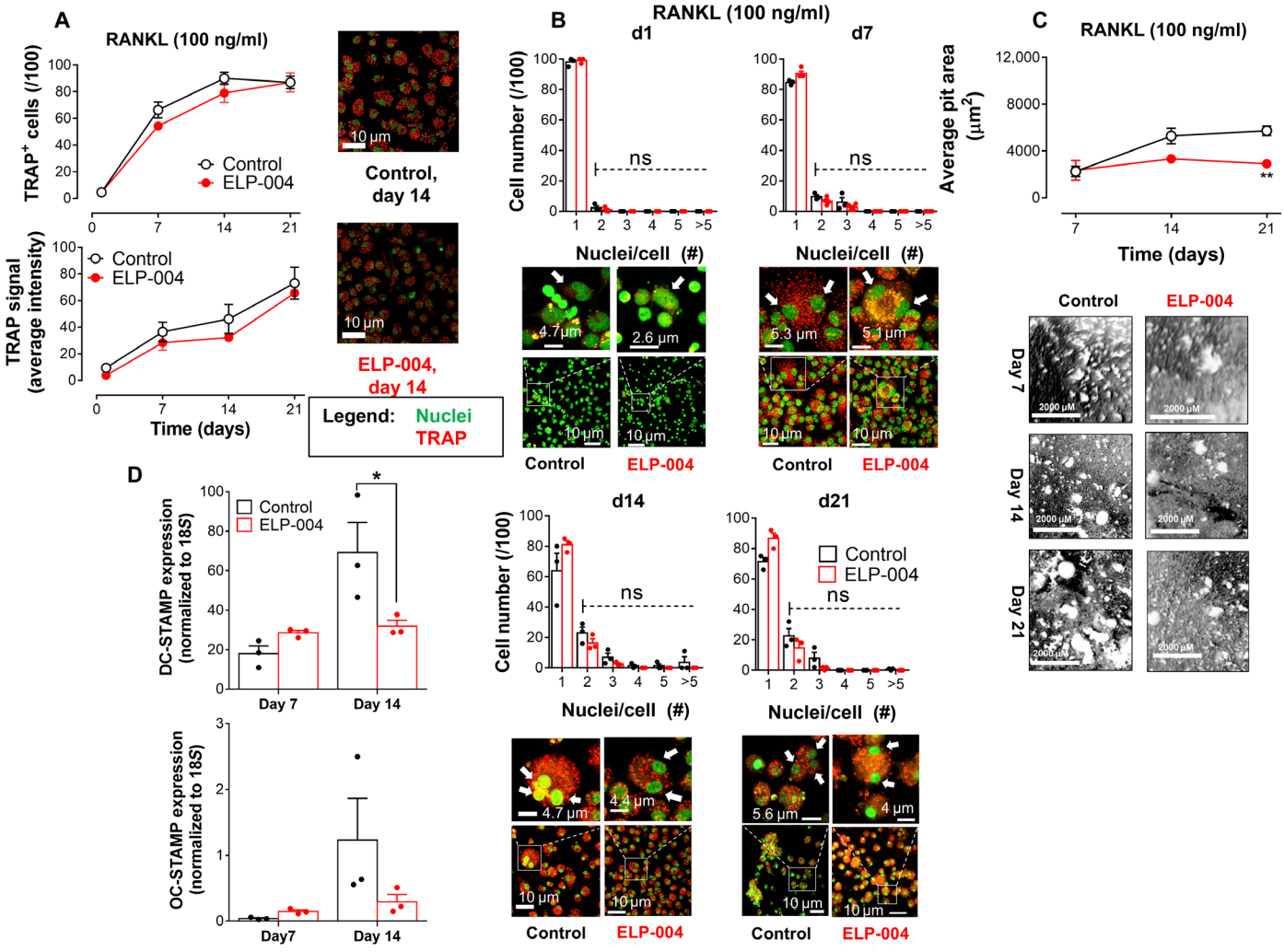

Fig. 3. ELP-004 has minimal effect on RANKL-induced osteoclastogenesis. Murine BMSMCs were grown for up to 21 days in media supplemented with mCSF (50 ng/ml) and RANKL (100 ng/ml) in the presence or absence of ELP-004 (100 nM). Each experiment was repeated a minimum of three times. Cells were fixed and stained for tartrate-resistant acid phosphatase (TRAP) activity at days 1, 7, 14, and 21. (**A**) Number (top) and intensity (bottom) of TRAP-positive osteoclast-like cells (of 100 cells) were counted for each time point; representative examples of TRAP-stained cells are depicted to the right. No significant changes in TRAP signal were observed. (**B**) At each time point, cells were also stained with 7-AAD to facilitate counting the number of nuclei per cell; multinucleation increased from day 1 to day 21 with no apparent effect of ELP-004. (**C**) RANKL-induced osteoclasts were grown on osteo-assay surface plates in the presence or absence of ELP-004 (100 nM). Pits formed by the resorptive activity of these osteoclasts were analyzed at days 7, 14, and 21, and the average pit sizes of 10 to 30 pits are shown along with representative images. Significant ELP-004–induced changes in pit sizes in RANKL-induced osteoclasts were observed at day 21 only [two-way ANOVA P(Interaction) = 0.0005]. $^{**}P < 0.01$. (**D**) BMSMCs were differentiated for 14 days in the presence of RANKL before extracting RNA at days 7 and 14 to measure DC-STAMP and OC-STAMP mRNA expression by qPCR. ELP-004 significantly inhibited increase in DC-STAMP expression at day 14; $^{*}P < 0.05$. Each experiment was repeated a minimum of three times with two technical replicates at each time point. ns, not significant.

ELP-004–induced decreases in multinucleation observed on days 7 and 14 (fig. S7B). Distinct from previously described conditions, ELP-004 had no effect on LTB4-induced increases in the expression of DC-STAMP and OC-STAMP (fig. S7C). Further, no significant changes in LTB4-induced expression of any other osteoclast markers screened were observed (fig. S8C). Last, LTB4 increased the ability of osteoclasts to degrade matrix in a manner similar to TNFα (Fig. 4C), with potent inhibition by ELP-004 observed (fig. S7D).

Together, these observations reveal that osteoclastogenesis exhibits enhanced sensitivity to ELP-004 in the presence of proinflammatory cytokines. Further, the examination of osteoclast markers reveals that ELP-004 specifically interferes with cell fusion, without significantly regulating the expression of other major osteoclast markers. In addition, it is important to acknowledge that, although ELP-004 strongly attenuated multinucleation and matrix degradation, ELP-004–treated mononuclear TRAP-positive cells retained some level of matrix degrading ability because small holes were observed (Figs. 3C and 4C, and fig. S7D); note that no holes were observed in a negative control (fig. S6C). Considering the essential role played by osteoclasts in Ca^{2+} homeostasis and bone maintenance, the fact that ELP-004–treated

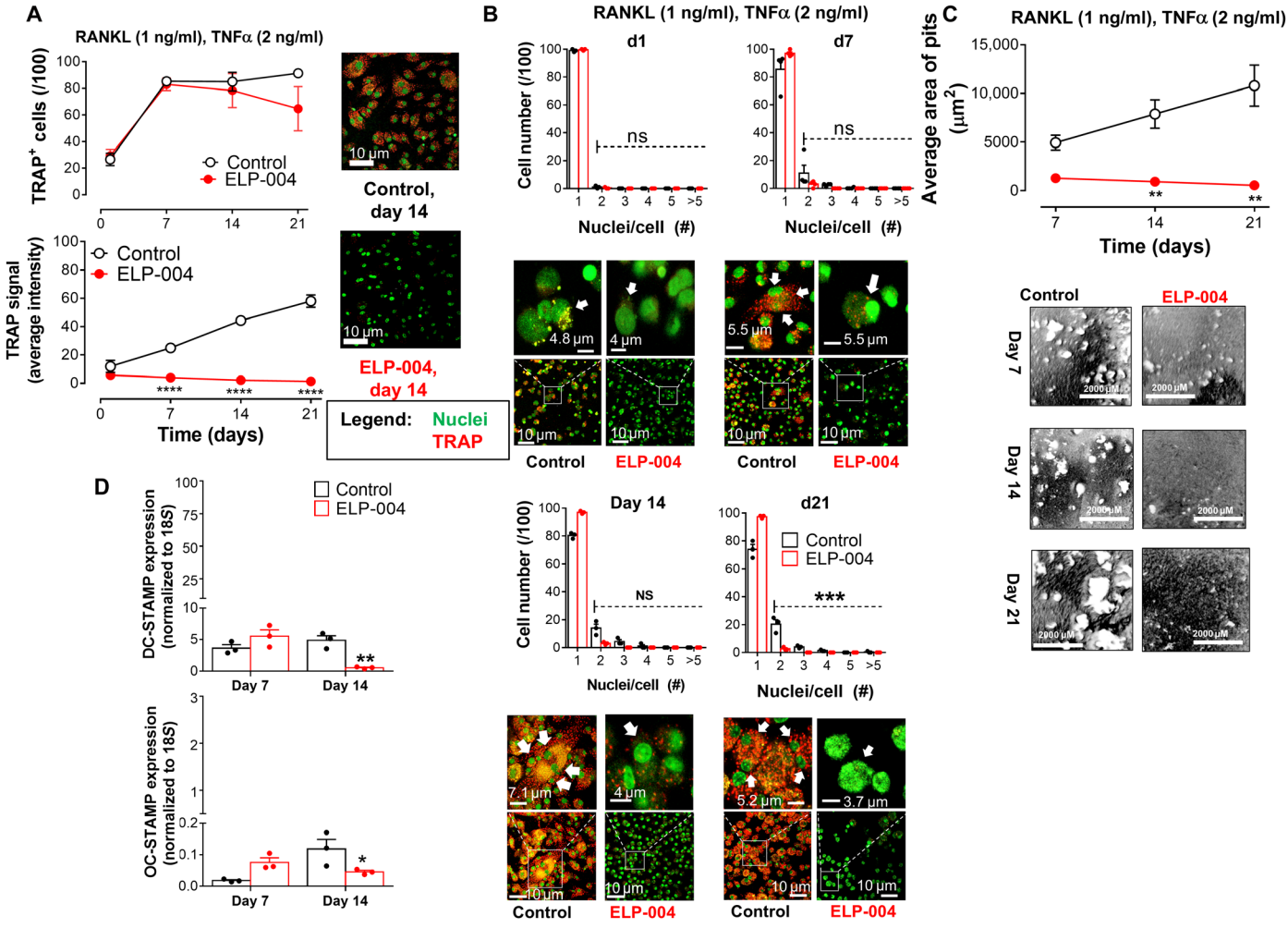

Fig. 4. ELP-004 blocks TNFα-induced osteoclast fusion. Murine BMSMCs were grown for up to 21 days in media supplemented with mCSF (50 ng/ml), RANKL (100 ng/ml), and TNFα (2 ng/ml) in the presence or absence of ELP-004 (100 nM). Each experiment was repeated a minimum of three times. Cells were fixed and stained for TRAP activity at days 1, 7, 14, and 21. (**A**) Number (top) and intensity (bottom) of TRAP-positive osteoclast-like cells (of 100 cells) were counted for each time point; representative examples of TRAP-stained cells are depicted to the right. ELP-004 had no effect on the number of TRAP-positive cells but significantly inhibited TRAP intensity [two-way ANOVA P(ELP-004) < 0.0001, P(time) < 0.0001, and P(interaction) < 0.0001]. (**B**) At each time point, cells were also stained with 7-AAD to facilitate counting the number of nuclei/cell; multinucleation increased from day 1 to day 21 in untreated, but not ELP-004–treated cells, as determined by two-way ANOVA with multiple comparisons; ***P < 0.001. (**C**) TNFα-induced osteoclasts were grown on osteo-assay surface plates in the presence or absence of ELP-004 (100 nM). Pits formed by the resorptive activity of these osteoclasts were analyzed at days 7, 14, and 21, and the average pit sizes of 10 to 30 pits are shown along with representative images. ELP-004 significantly inhibited pit formation for TNFα-induced osteoclasts [two-way ANOVA P(interaction) < 0.0001]. (**D**) BMSMCs were differentiated for 14 days in the presence of RANKL/TNFα before extracting RNA at days 7 and 14 to measure DC-STAMP and OC-STAMP mRNA expression via qPCR. ELP-004 significantly inhibited increase in both OC-STAMP [two-way ANOVA P(interaction) = 0.0051] and DC-STAMP [two-way ANOVA P(interaction) = 0.0017] expression. Each experiment was repeated a minimum of three times with two technical replicates at each time point. *P < 0.05, **P < 0.01, and ****P < 0.0001.

cells retain some capacity to degrade matrix is ideal for a potential therapeutic for the treatment of bone erosion.

The role of TRPC4 in osteoclastogenesis

The data described above demonstrate that ELP-004 blocks osteoclastogenesis induced by proinflammatory cytokines more effectively than that by RANKL alone. Because TRPC4 was the primary TRPC of which the expression was up-regulated under conditions of murine osteoclast differentiation (Fig. 1I), we tested the possibility that TRPC4 contributes to osteoclastogenesis driven by proinflammatory cytokines in a way that it does not with RANKL alone. Control (C57) and TRPC4$^{-/-}$ murine BMSMCs were collected to determine the contribution of TRPC4 to osteoclastogenesis. For comparison, osteoclastogenesis was also measured in TRPC(1–7)$^{-/-}$ murine BMSMCs (because these mice are outbred, they had a different control) to assess whether or not other TRPC channels could compensate for the loss of TRPC4. BMSMCs were differentiated into osteoclasts using RANKL, TNFα, or LTB4 for 14 days (Fig. 5 and fig. S9). While differentiation drove both TRAP activity and multinucleation in these cells, TRAP intensity and multinucleation were somewhat lower in this experiment (see Figs. 3 and 4 versus Fig. 5), potentially reflecting the fact that cells were freeze-thawed. Irrespectively, significant inhibition of multinucleation was observed for both TRPC4$^{-/-}$ and TRPC(1–7)$^{-/-}$ BMSMCs in the presence of either RANKL or RANKL/TNF (Fig. 5, A and B). For

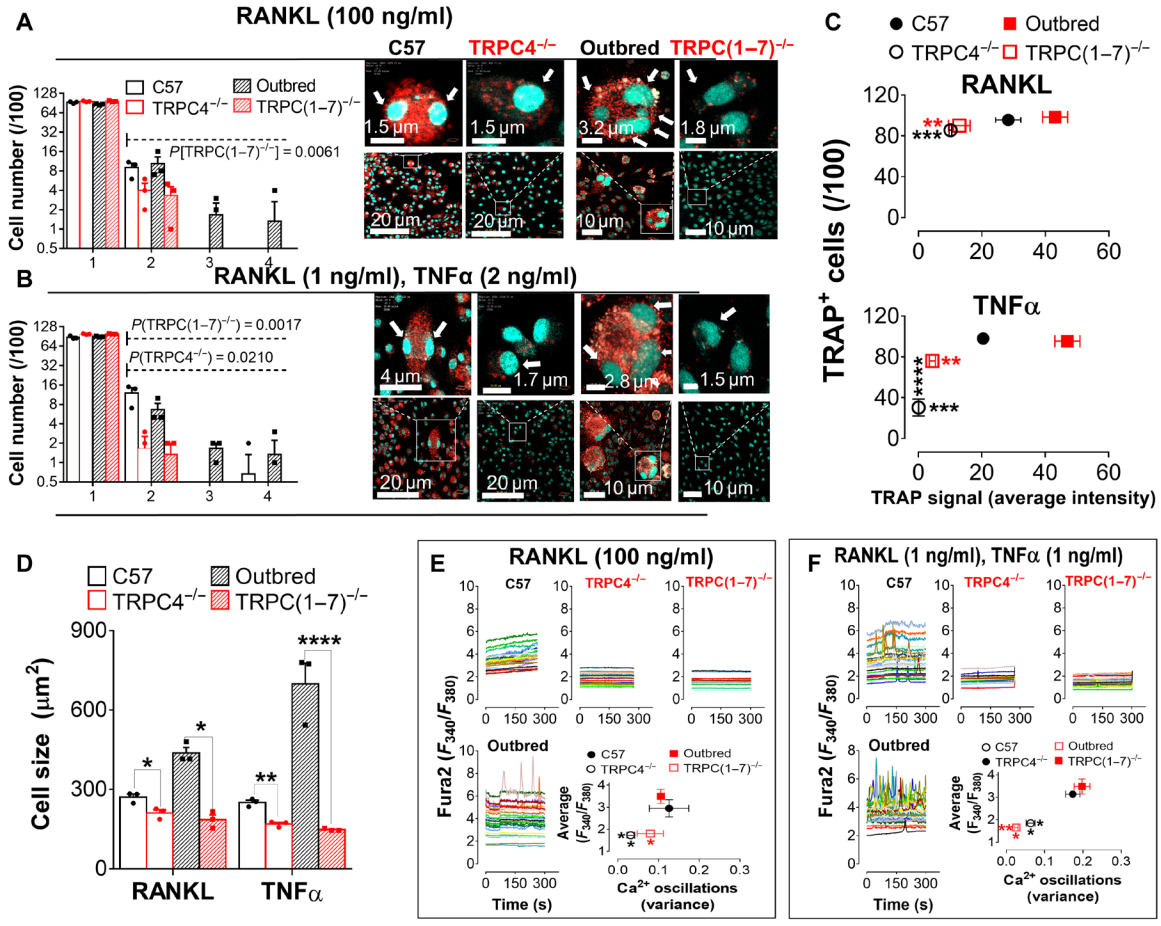

Fig. 5. TRPC4 is required for osteoclast maturation. BMSMCs collected from C57, TRPC4$^{-/-}$, outbred, and TRPC(1–7)$^{-/-}$ mice were differentiated for 14 days using mCSF (50 ng/ml) and RANKL (100 ng/ml) or mCSF (50 ng/ml), RANKL (1 ng/ml), and TNFα (2 ng/ml). C57 was control for TRPC4$^{-/-}$ samples, whereas outbred was control for TRPC(1–7)$^{-/-}$ samples. Data represent at least three biological replicates. (**A** and **B**) Cells were fixed and stained for TRAP activity; nuclei were marked with 7-AAD. The average number of nuclei per 100 cells is shown under each condition [unpaired *t* test comparing mononuclear and multinuclear cells; *P*(TRPC(1–7)$^{-/-}$, RANKL) = 0.0061; *P*(TRPC4$^{-/-}$, TNFα) = 0.0210; *P*(TRPC(1–7)$^{-/-}$, TNFα) = 0.0017]. (**C**) Frequency of TRAP-positive cells was plotted against TRAP signal intensity. The frequency was unaffected by loss of TRPC4 but was significantly lowered by loss of all seven TRPC channels when osteoclastogenesis was induced by TNFα only [two-way ANOVA *P*(interaction<0.0001)]. TRAP signal intensity was also significantly lower in TRPC4$^{-/-}$ and TRPC(1–7)$^{-/-}$ than controls when osteoclastogenesis was induced by both RANKL alone or TNFα [two-way ANOVA *P*(interaction) = 0.0076]. (**D**) Lack of TRPC4, similar to lack of all seven TRPC channels, significantly reduced cell sizes in both RANKL- and TNFα-driven osteoclasts [C57 versus TRPC4$^{-/-}$ two-way ANOVA *P*(cytokine treatment) < 0.0001; outbred versus TRPC(1–7)$^{-/-}$ two-way ANOVA *P*(interaction) = 0.0067]. (**E** and **F**) BMSMCs were plated on coverslips and loaded with Fura2 to measure basal Ca^{2+} concentration and oscillations. Average basal Ca^{2+} was measured for 30 to 100 cells in the same buffer for 3 to 5 min and plotted against Ca^{2+} oscillations alongside representative calcium traces for each condition. Both average basal Ca^{2+} and Ca^{2+} oscillations for both TRPC4$^{-/-}$ and TRPC(1–7)$^{-/-}$ cells were significantly lower than C57 or outbred cells, respectively, when driven by both (E) RANKL and (F) TNFα. **P* < 0.05, ****P* < 0.001, and *****P* < 0.0001.

LTB4-induced osteoclasts, the loss of multinucleation was only observed in TRPC(1–7)$^{-/-}$ BMSMCs (fig. S9A). TRAP intensity was notably higher in outbred mice; however, again, TRPC4$^{-/-}$ and TRPC(1–7)$^{-/-}$ BMSMCs exhibited significant decreases as compared to their respective controls after either RANKL or TNFα/RANKL treatment (Fig. 5C). Notably, decreased TRAP intensity was not observed in LTB4/RANKL-treated TRPC4$^{-/-}$ cells but observed in TRPC(1–7)$^{-/-}$ (fig. S9B). Further, the number of TRAP-positive cells was only changed in TNFα/RANKL-treated TRPC4$^{-/-}$ BMSMCs (Fig. 5C). TRPC4$^{-/-}$ BMSMCs were significantly smaller than their WT controls irrespective of treatment (two-way ANOVA; TNFα, $P < 0.02$; TRPC4$^{-/-}$, $P < 0.0001$). These differences were exaggerated considerably in TRPC(1–7)$^{-/-}$ cells [two-way ANOVA; interaction, $P < 0.01$; TNFα, $P < 0.03$; TRPC(1–7)$^{-/-}$, $P < 0.0001$], likely reflecting greater hypertrophy in outbred BMSMCs (Fig. 5D). Notably, differences in cell size were not observed when LTB4 was used in place of TNFα (fig. S9C), further demonstrating the specificity of specific aspects of osteoclastogenesis on cytokine-specific signals.

TRPC4$^{-/-}$ and TRPC(1–7)$^{-/-}$ BMSMCs exhibited lower intracellular Ca^{2+} levels under all three conditions of osteoclast differentiation (Fig. 5, E and F, and fig. S9D), although, again, the greatest effect was observed in the presence of TNFα/RANKL (Fig. 5F). Moreover, ELP-004 had no effect on intracellular Ca^{2+} in either RANKL or RANKL/TNFα osteoclasts derived from either

TRPC4$^{-/-}$ and TRPC(1–7)$^{-/-}$ BMSMCs (figs. S10 and S11, respectively). Moreover, neither TRPC4$^{-/-}$ nor TRPC(1–7)$^{-/-}$ BMSMCs incubated with RANKL- and/or TNFα-induced pit formation (fig. S12), suggesting that TRPC4 expression is essential to osteoclast function. To determine whether ELP-004 had TRPC-independent effects on osteoclastogenesis, all assays were repeated in its presence. However, ELP-004 had no effect on pit formation (fig. S12), TRAP expression (figs. S13A and S14A), multinucleation (figs. S13B and S14B), or cell size (figs. S13C and S14C).

These data reveal a previously unidentified role for TRPC4 in osteoclastogenesis. While multiple parameters of osteoclastogenesis were affected under all conditions, TNFα-/RANKL-induced osteoclastogenesis was consistently the most sensitive to the loss of TRPC4 expression. Because TRPC(1–7)$^{-/-}$ cells did not exhibit any greater loss of osteoclastogenesis than TRPC4$^{-/-}$ cells, the contribution of any other TRPC channels to murine osteoclastogenesis can be discounted. Further, because ELP-004 treatment did not have any additional effects when osteoclasts were induced to form from TRPC4$^{-/-}$ and TRPC(1–7)$^{-/-}$ BMSMCs, we conclude that TRPC4 is required for inhibition of osteoclastogenesis by ELP-004.

Lipid-based ELP-004 delivery system reaches target tissues at sufficient levels for treatments

Bone erosion is a progressive feature of RA which is caused by a disbalance between bone-forming osteoblasts and bone-resorbing osteoclasts. Specifically inhibiting proinflammatory osteoclastogenesis without inhibiting RANKL-dependent bone destruction required in bone maintenance would allow for long-term treatment and improve options available to patients with RA or other bone-destructive diseases. We have previously demonstrated that a small-molecule, 3,4-dichloropropionanilide, reduces arthritis in a collagen-induced arthritis (CIA) mouse model when administered beginning at the time of arthritis induction (*27*); however, 3,4-dichloropropionanilide is metabolized into two immunotoxic intermediates (*40*–*44*), which produce toxicities independent of its function (*41*). We sought to develop a derivative of 3,4-dichloropropionanilide with reduced toxicities and equal efficacy in reducing bone erosion in arthritis. Extensive pharmacokinetic and metabolism analyses of ELP-004 were conducted including off-target receptor engagement, cardiotoxic and genotoxic (DNA mutations and chromosomal abnormalities) assessments, cytochrome P450 induction and inhibition, blood-brain barrier permeability, T cell viability, and assessment of overt neurological side effects (at doses ~2 to 60× higher than presented in the current manuscript) with minimal to no adverse findings (*29*).

Here, we assessed the efficacy of ELP-004 in a mouse model of arthritis. To minimize the total dose needed for efficacy and shield the drug from binding to serum proteins, ELP-004 was combined with poly(lactic-*co*-glycolic acid) (PLGA) and formulated in a high concentration (30 mg/ml) lipid nanoemulsion (ELP-004–LNE) for oral administration or a low concentration (1 mg/ml) lipid nanoparticle (ELP-004–NP) for daily intraperitoneal injections (fig. S15A). Physical parameters, including particle size and zeta potential, of the lipid formulations were similar between the two with ELP-004–LNE particles being larger than the low-concentration ELP-004–NP; in addition, particle size remained consistent over 5 weeks, indicating stability with long-term storage at 4°C (fig. S15, B to D). The entrapment efficacy of ELP-004–NP was found to be 52%. These data are consistent with previous studies using this delivery system (*45*), suggesting that our formulations were sufficient for in vivo assessment.

We then evaluated the ability of ELP-004 to reach the target sites of plasma and bone marrow at 5, 30, 45, 60, and 360 min after a single intraperitoneal dose of ELP-004–NP (4 mg/kg). The plasma reached a maximum concentration (C_{max}, 1199 ± 581.5 ng/ml or 4.8 ± 2.5 μM) at 5 min, while the bone marrow C_{max} of 66.28 ± 22.75 ng/ml (285 ± 98 nM) occurred at 30-min post-dose (fig. S15E). Because oral administration is preferred by patients over therapies administered by injection or infusion, we also assessed the tissue distribution of ELP-004 in the plasma, bone marrow, spleen, kidney, visceral adipose tissue, heart, liver, muscle (gastrocnemius), and brain at 15 min or 1 hour following oral gavage of a single dose of ELP-004–LNE (180 mg/kg) in DBA1/J mice. Mean plasma concentrations of ELP-004 were 1517.06 ng/ml (6.54 μM) at 15 min and 2078.22 ng/ml (8.95 μM) at 1 hour, while bone marrow concentrations reached 178.0 ng/ml (766.9 nM) and 186.6 ng/ml (803.7 nM), respectively (fig. S15F). ELP-004 was detectable in all tissues tested at relatively consistent concentrations at both 15 min and 1 hour after oral administration, with the highest levels observed in the visceral adipose tissue, suggesting it is rapidly adsorbed, circulated throughout the body, and may preferentially distribute to the fat (fig. S15G). The brain-to-plasma ratio of ELP-004 was 0.76 at 15 min and 0.68 at 1 hour, suggesting no specific enrichment in the brain. No overt behavior toxicities were observed in either formulation/route of administration. Overall, these data are compelling to suggest that lipid-based delivery of ELP-004 is safe for both intraperitoneal and oral administration in mice and that ELP-004 may reach therapeutic levels at bone target sites.

ELP-004 reduces bone erosion in a mouse model of RA

To evaluate the efficacy of ELP-004 in the reduction of bone erosion in vivo, we used a mouse model of RA. "SKG mice," originally described by Sakaguchi *et al.* (*46*), are BALB/c mice that have a natural mutation in the *Zap70* gene encoding a component of the T cell receptor. The point mutation reduces, but does not abolish, T cell receptor signal transduction thereby allowing self-reactive T cells to escape negative selection in the thymus and reach the peripheral T cell pool, skewing the T cell repertoire toward self-reactivity (*47*). The SKG arthritis model was selected because it mimics human disease in several ways including female sex bias, extra-articular manifestations and presence of rheumatoid factor, and antibody against collagen type II (*46*).

Male and female SKG mice were induced with RA at 8 weeks of age using a single dose of zymosan A (2 mg), which causes measurable arthritis in all animals (*48*) and, consistent with human disease, produces more profound disease in female than male mice (*48*, *49*). The arthritic indices in all four paws were assessed weekly (Fig. 6A). Our ability to assess arthritis development in this model relies on physical swelling, severe redness, and joint malformation in the paws. However clinically, patients are likely to report joint pain consistent with arthritis to their general physicians before being referred to a rheumatologist. Bone erosions develop early in the course of RA and progressively result in permanent joint damage and physical malformations [reviewed in (*50*)]. To mimic an early treatment paradigm, beginning on day 3, mice were treated by daily oral gavage with ELP-004–LNE (180 mg/kg) for 8 weeks; no overt toxicities, including lethargy or hyperactivity, were observed. The treatment did not alter

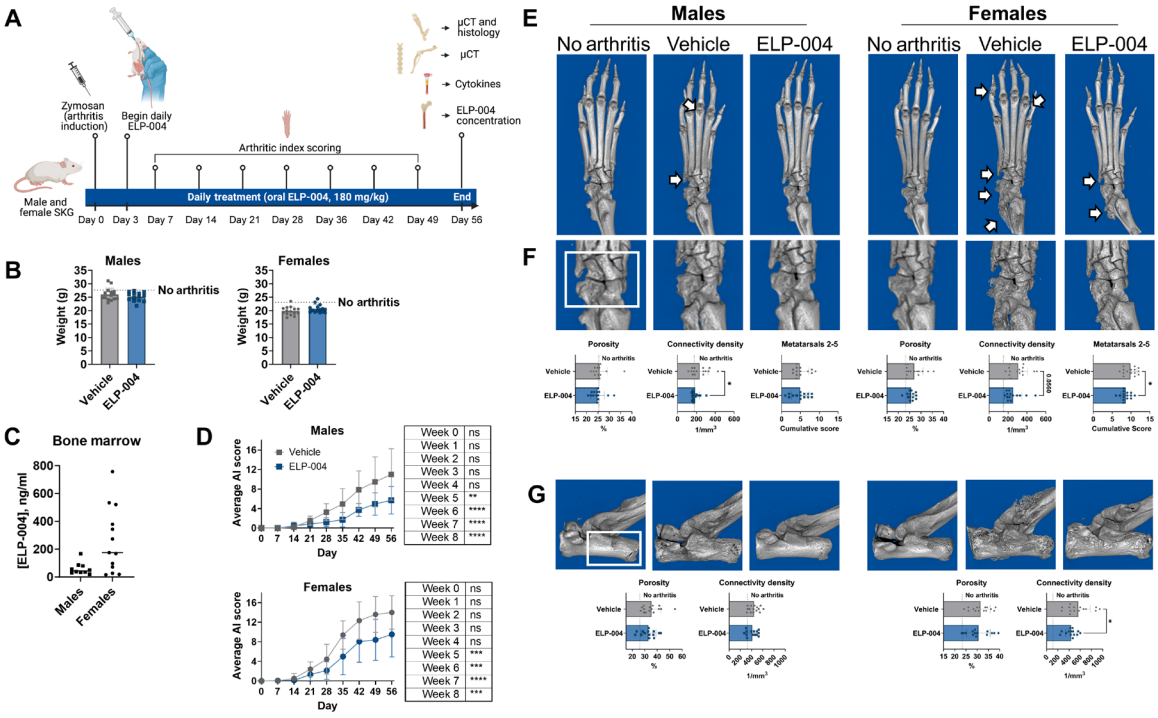

Fig. 6. Daily oral treatment with ELP-004–LNE reduces arthritis phenotypes in SKG mice. (**A**) Schematic representation of experimental design. Arthritis was induced in male and female SKG mice with a single dose of 2 mg of zymosan. Beginning on day 3 after induction, mice were treated daily with ELP-004–LNE (180 mg/kg) or vehicle via oral gavage. The arthritic index (AI) was assessed weekly by scoring each paw individually on a scale of 0 to 4: 0, normal; 1, mild, but definite redness and swelling limited to individual digits; 2, two swollen joints/digits; 3, three or more swollen joints/digits; and 4, severe swelling of all joints/digits. All paws were evaluated; maximal AI per mouse was 16. The study was ended on day 56, which was 24 hours after final ELP-004–LNE dose. Blood, rear legs/paws, and spine were collected from each mouse for analyses. $n = 14$ to 15 per sex and treatment. (**B**) Total body weight on d56 was unaffected by treatment. (**C**) Concentration of ELP-004 was measured in the bone marrow to assess concentrations at the site of target engagement. Bone marrow was isolated from the femur and tibia 24 hours after the final treatment. (**D**) Weekly AI assessments were analyzed using a repeated-measures two-way ANOVA with Šídák's correction for multiple comparisons. (**E**) The left hind paw of each mouse was assessed by microCT. Examples of bone erosion indicative of arthritis are indicated by white arrows. (**F** and **G**) Porosity and pore connectivity density of the tarsus (F) and calcaneus (G) (shown in white boxes) were quantified in each mouse. Cumulative erosion scores of metatarsals are quantified on the right (F). Vehicle- and ELP-004–treated animals were compared using a one-tailed, unpaired *t* test, or Mann-Whitney, when appropriate. $^{*}P < 0.05$, $^{**}P < 0.01$, $^{***}P < 0.001$, and $^{****}P < 0.0001$.

gross or liver weights, while it resulted an increase in splenic weight in female but not male mice (Fig. 6B and fig. S16A). Plasma cytokines were unchanged between treated and untreated mice (fig. S16B). Together, these data suggest that daily oral treatment does not grossly alter immune cell composition and function and is safe for long-term administration in mice.

Next, the concentration of ELP-004 was measured in the bone marrow to assess compound concentrations at the site of potential target engagement. Bone marrow was isolated from the femur and tibia 24 hours after the final treatment, and ELP-004 levels were measured at 256.6 ng/ml (1.11 μM) and 1121 ng/ml (4.83 μM) in males and females, respectively. Not only did females have a higher concentration in the bone marrow, but the range of measured concentrations was larger in females [95% confidence interval (CI), 2.20 to 7.46 μM] than in males (95% CI, 0.53 to 1.68 μM) (Fig. 6C). In addition, because these levels were detected 24 hours after the final dose, the data suggest that oral administration of ELP-004–LNE prolongs the presence of ELP-004 in vivo and that the drug may accumulate in the target tissues despite pharmacokinetic assessment indicating rapid elimination (fig. S15E). ELP-004 is below the limit of detection in the plasma when assessed at the same time point. Regardless of the differences in ELP-004 concentration, both male and female ELP-004–treated mice had reduced arthritic indices beginning at week 5 as compared to the vehicle controls (Fig. 6D), suggesting efficacy in reducing swelling at both concentrations. Unexpectedly, the treatment only showed a trend to reduce joint inflammation in paws without reaching statistical significance in either sex (fig. S16C); therefore, we concluded that ELP-004 reduces edema or overall inflammation in paws rather than specific inflammation within the joint.

To assess whether ELP-004 reduces bone erosion associated with RA, we imaged the paws, femurs, and spines from each mouse using microcomputed tomography (microCT or μCT; Figs. 6, E to G, and 7, and fig. S17). Visual areas of bone erosions were observed in the arthritic paws of vehicle controls, with the ELP-004 treatment bringing obvious improvement in females (Fig. 6E, white arrows). This is consistent with previous reports suggesting that more severe disease occurs in female mice in this model (*49*), and regions most often eroded in the paws include the metatarsals of digits 2 to 5 and tarsus (or ankle). We examined the tarsus and calcaneus separately as the latter is easy to separate from surrounding bones and erosions in the calcaneus are associated with arthritis in the mouse (*51*, *52*). Using three-dimensional (3D) analysis software, we sectioned the tarsus (Fig. 6F, white box) and calcaneus (Fig. 6G, white box) and assessed

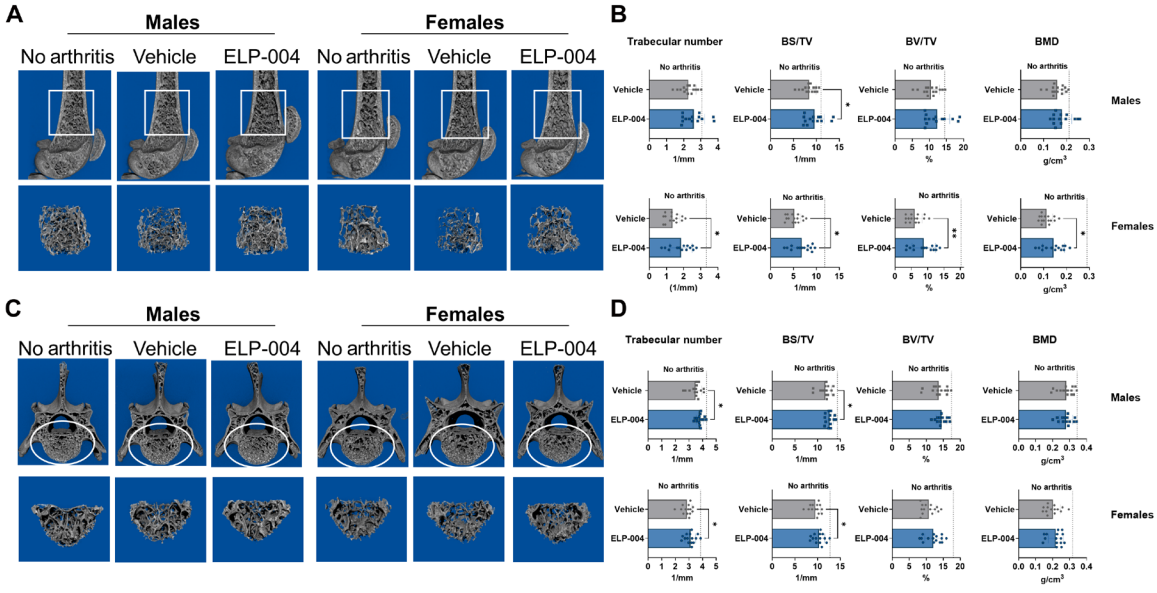

Fig. 7. ELP-004–LNE improves bone structure parameters in the SKG mouse model of arthritis. (**A**) Femurs and (**C**) L5 vertebrae in the spine were visualized using μCT. The trabecular bone analyzed in the region of interest (white box) is depicted below. Microarchitecture parameters were quantified in the femurs (**B**) and spines (**D**). Vehicle- and ELP-004–treated animals were compared using a one-tailed, unpaired *t* test, or Mann-Whitney, when appropriate. *$P < 0.05$.

porosity (% pore volume per total volume) and connectivity density of the pores (which quantifies the number of connections that occur between pores in a volume of space—meaning that the higher the connectivity density, the less dense the bone is). As expected through visual inspection of the paws, after RA induction, the porosity and connectivity density in the calcaneus appeared to be increased in both sexes compared to the no arthritis controls, with the increases in the females more robust than in males. However, while the no arthritis controls are included on the graphs (dashed line) to show where normal mice fall for each parameter, they were not included in the formal analyses due to fewer mice ($n = 2$ to 3) in each assessment. Compared to the calcaneus, tarsi exhibited less robust changes, displaying moderate increases in connectivity density in the males, whereas both porosity and connectivity density were altered in females. While the ELP-004 treatment did not significantly change the porosity in the tarsus or calcaneus in either sex, it attenuated the increase in the connectivity density in the tarsus of males ($P < 0.05$) (Fig. 6F) and that in the calcaneus of females ($P < 0.05$) (Fig. 6G). There was also a strong tendency for ELP-004 to rescue connectivity density of the pores in tarsus of female animals ($P = 0.056$) (Fig. 6F). Together, these results suggest strengthening of the bone structures by ELP-004 in the tarsus of males, and perhaps also females, and in the calcaneus of females (Fig. 6G). Last, to assess the erosions in the metatarsals, we scored each bone on a scale of 0 to 3, where 0 = normal and 3 = full-thickness holes. Comparison of the cumulative scores for metatarsals 2, 3, 4, and 5 (maximum score = 12) revealed that ELP-004 reduced erosions in female ($P < 0.05$), but not male, mice (Fig. 6F).

Osteoporosis is one of the most common extra-articular complications of RA and is characterized by decreased bone mineral density (BMD) and increased risk of fractures. The latter is estimated to occur in about 27.6% of patients with RA, which approximately doubles the rate in the general population (*53*). In the United States, osteoporotic fractures account for about one-third of RA-related mortality (*54*). In mouse models, trabecular microarchitecture in the long bones and spine is a measurement of bone integrity. We assessed the trabecular bone in the femur and L5 vertebrae in the spine using μCT (Fig. 7, A and C, white outlined areas represent the trabecular bone selected for analysis, bottom panels). Quantification of microarchitecture parameters revealed that ELP-004–treated female mice had increased trabecular number, bone volume/tissue volume (BV/TV), and BMD in the femurs compared to vehicle-treated controls (Fig. 7B), indicating increased bone integrity with the treatment. Bone surface density (BS/TV) was used to measure surface roughness/erosion (*51*). The lower BS/TV values observed in the vehicle groups (males: $8.43 \pm 1.49\ mm^{-1}$, females: $5.15 \pm 1.49\ mm^{-1}$) than in the ELP-004–treated mice (males: $9.60 \pm 2.16\ mm^{-1}$, females: $6.78 \pm 2.20\ mm^{-1}$, $P < 0.05$) suggest that ELP-004 significantly ameliorated bone erosion/roughness. Trabecular number and bone surface density were also increased in the L5 vertebrae of ELP-004–treated mice compared to vehicle controls in both sexes (Fig. 7D). Together, the trabecular parameters indicate the 8-week daily oral treatment with ELP-004–LNE curtailed bone integrity deterioration in RA.

Similar studies were also performed with a low-dose ELP-004–NP formulation delivered daily by intraperitoneal injection (6 mg/kg for 8 weeks beginning 3 days after induction). However, this dose and route of administration lacked the effects found with the oral formulation (figs. S18 to S20). Our pharmacokinetics (PK) data (fig. S15, E and F) suggest that the intraperitoneal formulation resulted in lower ELP-004 concentrations than the oral formulation in the plasma and bone marrow and sustained levels (over 1 hour) following the oral dose, which was not observed in the bone marrow following intraperitoneal administration. Therefore, we hypothesize that the difference in effectiveness is due to both increased concentrations of ELP-004 and longer duration in the bone marrow compartment following oral dosing. No differences were observed in total or organ weights (figs. S18B and S19A), and inflammation appeared

unchanged with the treatment as indicated by arthritic indices, joint inflammation, and plasma cytokines (figs. S18C and S19, B and C). To test whether T cell function or immune phenotypes were altered by the low-dose ELP-004–NP in vivo, we measured secreted cytokines after ex vivo T cell activation (fig. S19D) and quantified total leukocytes (fig. S19E) along with proportions of immune cell populations in the spleen (fig. S19F), observing no differences. Visual inspection of the paws suggested that bone erosions might be diminished by ELP-004–NP (6 mg/kg via i.p.), showing meaningful trends in reducing porosity in the tarsus ($P = 0.0950$ for males and $P = 0.0676$ for females) and preventing erosions in the metatarsals of females ($P = 0.0525$) (fig. S18, D and E). However, minimal, if any, changes were observed in the calcaneus, femurs, or spine parameters (figs. S18F and S20).

Overall, the in vivo studies in mice reveal that ELP-004 is a promising compound for the treatment of bone erosion associated with RA. The data suggest that a lipid-based, oral formulation can be safely administered to mice without overt toxicities and that ELP-004 is effective at suppressing erosions when administered after arthritis induction in our model. Cumulatively, these data suggest that the improvements are more pronounced in the females; however, there is larger variability within the data, which is consistent with the variability observed in ELP-004 concentration in the bone marrow. Future studies will determine whether there are limits to how late in the development of RA the drug can be added to get a measurable effect. However, further optimization of the delivery system may be necessary to observe maximal reduction of RA-associated bone erosions.

ELP-004 inhibits osteoclastogenesis in human cells

The data described above reveal ELP-004 as a potential therapeutic for the treatment of arthritis-induced bone erosion. To assess whether it is also able to interfere with human osteoclastogenesis, we used PBMCs obtained from four anonymous blood donors by Temple University Hospital (Philadelphia, PA). While we (*5*) and others (*55*, *56*) have studied human osteoclastogenesis using RANKL, this study is the first to assess the ability of TNFα to contribute to this process. Human PBMCs were incubated in mCSF alone (control), mCSF and RANKL (100 ng/ml) or mCSF, RANKL (1 ng/ml), and TNFα (2 ng/ml) for 14 days. TNFα-/RANKL-induced osteoclasts exhibited considerably more Ca^{2+} oscillations than cells incubated with RANKL alone (Fig. 8, A and B; individual patient data in fig. S21, A to D). Furthermore, although TNFα had no effect on the average basal intracellular Ca^{2+} levels in the absence of ELP-004, the drug significantly lowered basal Ca^{2+} levels under both conditions, with the decrease being more pronounced in cells incubated with TNFα (Fig. 8, A and B). Similar to that observed with mouse cells, ELP-004 significantly inhibited multinucleation under all conditions, with the effect being more robust in the presence of TNFα (Fig. 8, C and D). Moreover, ELP-004 curtailed the increases in TRAP-positive cells and TRAP intensity in these cells (Fig. 8E; individual patient data in fig. S21, E to H). ELP-004 only attenuated the increase in osteoclast size in cells incubated with TNFα (Fig. 8F), again demonstrating that ELP-004 preferentially affects osteoclastogenesis induced by proinflammatory cytokines. Last, we assessed TRPC expression in PBMCs (Fig. 8G). Unexpectedly, unlike in mouse cells, the only TRPC expressed by human osteoclasts and macrophages was TRPC1, with significantly more expression in osteoclasts detected at the mRNA level (Fig. 8G). While we were surprised by the interspecies difference in TRPC expression, prior studies have also shown TRPC1 to be both expressed (*20*, *26*, *57*) and required for osteoclast maturation (*57*). Given the high potency of ELP-004 as an inhibitor of all tested members of the TRPC family (Fig. 1), these findings imply that ELP-004 inhibits human osteoclastogenesis (particularly in the presence of proinflammatory cytokines) by targeting TRPC1 instead of TRPC4. However, future investigations are needed to fully understand TRPC channel expression at the protein level during osteoclastogenesis and to define how the presence of TRPC1 affects sensitivity to inhibition by ELP-004.

DISCUSSION

In the current study, we demonstrated that ELP-004 inhibits TRPC channel–mediated Ca^{2+} entry with high potency, which, in turn, preferentially inhibits inflammatory cytokine-induced pathological osteoclastogenesis in both murine and human models. This included blockade of intracellular Ca^{2+} concentration increase, inhibition of NFATc1 nuclear localization, TRAP expression, multinucleation, and matrix resorbing ability. We further established that TRPC4 is the primary TRPC expressed in murine osteoclasts, distinct from human osteoclasts that primarily express TRPC1. Using cells obtained from $TRPC^{-/-}$ mice, we established that TRPCs are required for osteoclastogenesis and that their deletion inhibits osteoclastogenesis in a manner similar to the treatment by ELP-004. Considered collectively, these data reveal ELP-004 as a TRPC family inhibitor with potent effects on osteoclastogenesis particularly in the presence of proinflammatory cytokines.

Bone homeostasis is maintained by the function of bone-resorbing osteoclasts and bone-forming osteoblasts. In this study, we compared physiological RANKL-induced osteoclastogenesis with osteoclastogenesis driven primarily by LTB4 and TNFα. While osteoclastogenesis occurred similarly under these conditions, we observed differential sensitivity to ELP-004. In the context of RA, inflammatory cytokines such TNFα can increase inflammation by stimulating PLA2, the activity of which has been reported to increase in RA patients' serum (*12*, *58*, *59*). TNFα, particularly, has received attention as a therapeutic target for RA due to having an apex position in the proinflammatory cytokine cascade and being involved in the pathogenicity of several autoimmune disorders (*32*, *60*). The ability of TNFα to drive osteoclastogenesis in the presence of low dose RANKL has been demonstrated previously (*9*, *31*, *61*–*64*), although the current study is the first to examine a role for ELP-004 or demonstrate differences in cytosolic Ca^{2+} levels. In addition, this is the first demonstration that LTB4 can also serve this role in osteoclastogenesis; whether or not other proinflammatory cytokines can also serve this role remains unknown. Because TNFα induces LTB4 production (*11*–*13*), and LTB4 can stimulate TNFα release (*10*), it is possible that one of LTB4 or TNFα is the true mediator of osteoclastogenesis, although it is also possible that the LTB4 and TNFα signaling pathways induce osteoclastogenesis via a common mediator. NF-κB is a central mediator of both RANK (*65*) and TNFα (*66*) signaling, but how LTB4 might engage NF-κB is less clear. On the other hand, Ca^{2+}-dependent NFAT engagement is critical for osteoclastogenesis; how either RANK or TNFα might stimulate a Ca^{2+} response remains elusive. Hence, it seems most likely that RANKL, TNFα, and LTB4 could all contribute to osteoclastogenesis independently through distinct but overlapping pathways.

Ca^{2+} signaling is crucial for NFATc1 activation via both direct binding and Ca^{2+}/calcineurin-dependent dephosphorylation (*36*).

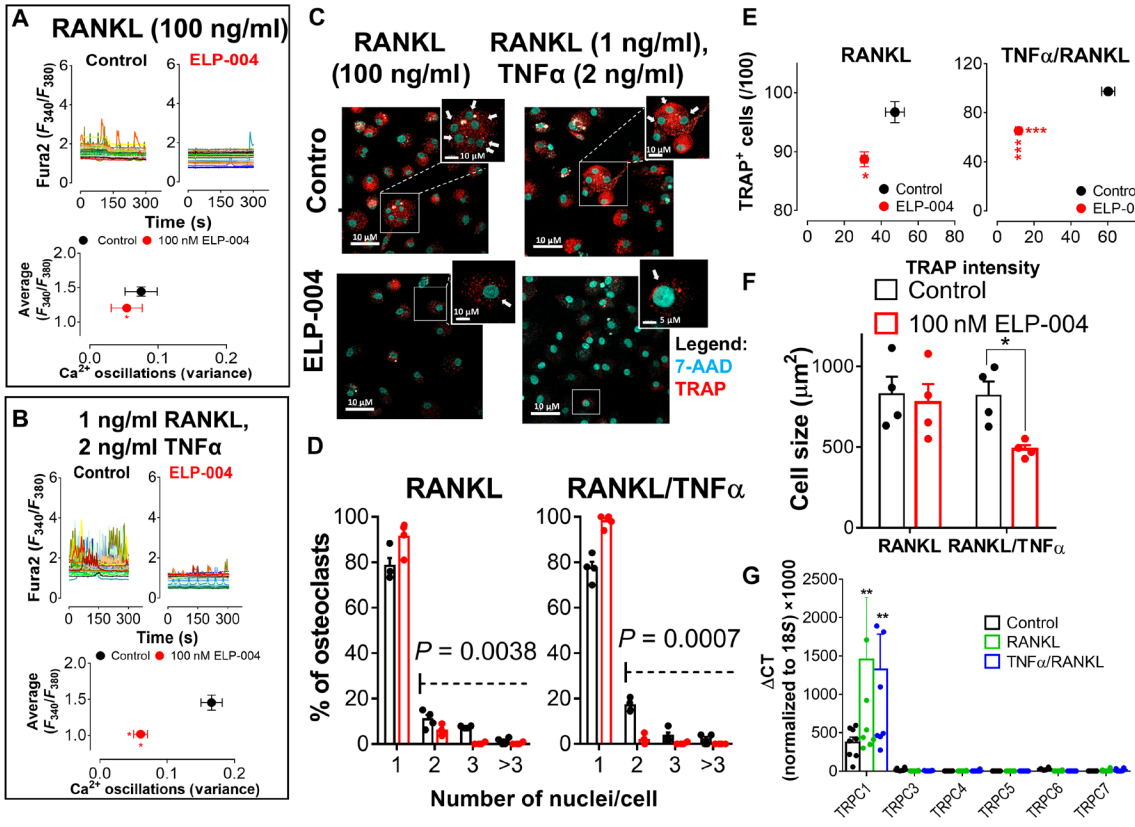

Fig. 8. ELP-004 inhibits human osteoclastogenesis. Human PBMCs from four patients were incubated in media supplemented with (i) mCSF (50 ng/ml; control); (ii) mCSF (50 ng/ml) and RANKL (100 ng/ml); or (iii) mCSF (50 ng/ml), RANKL (1 ng/ml), and TNFα (2 ng/ml) ± ELP-004 (100 nM). (**A** and **B**) Human osteoclasts plated on coverslips were loaded with Fura2 after 14 days of growth. Average basal Ca^{2+} was measured for 30 to 50 cells in the same buffer for 3 to 5 min was plotted against variance for each condition. In RANKL alone, ELP-004 lowered average basal Ca^{2+} (unpaired *t* test, $P = 0.0486$) but had no effect on Ca^{2+} oscillations [(A)]. ELP-004 significantly lowered both average basal Ca^{2+} (unpaired *t* test, $P = 0.0330$) and Ca^{2+} oscillation generation (unpaired *t* test, $P = 0.0189$) cultured in TNFα/RANKL [(B)]. Asterisks on the *x* axis denote comparison of Ca^{2+} oscillation generation, whereas those on the *y* axis denote comparisons of average basal Ca^{2+}. (C to F) Cells were fixed and stained for TRAP and 7-AAD after 14 days of growth. (**C**) Representative images. (**D**) Nuclei were stained with 7-AAD; multinucleation was inhibited by ELP-004 treatment in both RANKL- and TNFα-induced osteoclasts [unpaired *t* test, *P*(ELP-004, RANKL) = 0.0038; *P*(ELP-004, TNFα) = 0.0007]. (**E**) ELP-004 inhibited the number, but not intensity of $TRAP^+$ cells driven by RANKL (unpaired *t* test, $P = 0.0222$); both the number (unpaired *t* test, $P = 0.00050$) and intensity (unpaired *t* test, $P = 0.0001$) of $TRAP^+$ cells were inhibited in the presence of TNFα; asterisks on *y* axis denote comparison in TRAP intensity, whereas those in *y* axis denote comparison in $TRAP^+$ cell count. (**F**) ELP-004 treatment significantly reduced cell size in TNFα-induced osteoclasts only ($N = 3$). (**G**) qPCR reveals TRPC1 expression only, with up-regulation in both RANKL- and TNFα-induced osteoclasts compared to macrophages. $^*P < 0.05$, $^{***}P < 0.001$, and $^{****}P < 0.0001$.

We have shown that the rise in cytosolic Ca^{2+} levels through either TRPC- or Orai-mediated Ca^{2+} entry is essential for NFATc1 translocation during osteoclastogenesis. The role of store-operated Ca^{2+} signaling in RANKL-induced physiological osteoclastogenesis has been previously established (*5*–*7*, *27*, *67*–*69*). How these Ca^{2+} signals are stimulated via these receptors remains somewhat unclear, although c-Fos and to a certain extent, TNF receptor–associated factor 6 signaling pathways have been shown to play important roles in RANKL-induced NFATc1 activation during osteoclastogenesis (*70*). The activity of c-Fos is modulated by STIM1/Orai-mediated Ca^{2+} signal and the local Ca^{2+} environment created by SOCE is crucial for c-Fos activation (*21*, *71*). In particular, c-Fos up-regulation in RBL-1 cells is uniquely dependent on Orai-mediated Ca^{2+} entry, distinct from global Ca^{2+} changes (*72*). Hence, c-Fos expression would not be expected to be TRPC dependent. RANKL, although the mechanisms were not made clear, has been shown to drive long-lasting increases in reactive oxygen species (ROS) and intracellular Ca^{2+} oscillations (*69*, *71*) during osteoclastogenesis (*69*). This pathway was shown to include RANKL-mediated Rac1 stimulation to generate ROS, which stimulates PLCγ1 and leads to STIM1-regulated intracellular Ca^{2+} oscillation. However, given the lack of effect of ELP-004 on RANKL-induced Ca^{2+} content or osteoclastogenesis, this mechanism may be specific to physiological osteoclastogenesis and not entirely relevant to arthritis.

This is the first demonstration that pathological osteoclastogenesis mediated by inflammatory cytokines such as TNFα and LTB4 uses Ca^{2+} signaling mechanisms different from that of physiological osteoclastogenesis. TRPC4 is typically activated by coincident stimulation of both $G_{q/11}$-PLCβ and $G_{i/o}$ proteins (*73*, *74*). LTB4 would be expected to activate TRPC4 by fulfilling both requirements via its receptors BLT1 and BLT2, both found in osteoclast precursors (*75*). Given the previously cited relationship between TNFα and LTB4 (*10*–*13*), it is possible that LTB4 mediates TNFα-induced TRPC activation, although TNFα was more effective than either LTB4 or RANKL alone as an inducer of osteoclastogenesis, suggesting unique features of TNFα signaling. For example, in human endothelial cells, TNFα

activates TRPC1 via an NF-κB–dependent pathway (*76*). Moreover, in rat cardiomyocytes, prolonged exposure to TNFα leads to decreased synthesis of the phospholipid phosphatidylinositol, the precursor of PIP_2, which would be expected to enhance TRPC4 activity. Mace *et al.* (*77*) showed that TRUSS (TNFα receptor ubiquitous signaling and scaffolding protein), or TRPC4-associated protein, links TNFR1 with TRPC1/4/5, but not with the TRPC3/6/7 subfamily of TRPC channels in HEK293 cells. This association among TRUSS, TNFR1, and TRPC4 (in murine osteoclasts) or TRPC1 (in human osteoclasts) could also facilitate channel activation; future studies linking TNFR1 to TRPC channels may validate these being other potential mechanisms of TNFα-induced Ca^{2+} elevation during osteoclastogenesis.

The role of TRPC4 has been studied in several cell types in both mice and humans where it promotes cell proliferation and migration (*78*, *79*), but its involvement in osteoclastogenesis has not been previously described in vivo. Moreover, the fact that $TRPC4^{-/-}$ BMSMCs exhibited severe defects in osteoclastogenesis, particularly when induced by TNFα, is consistent with our hypothesis that TRPC4 is the sole TRPC channel expressed in murine osteoclasts. This was reflected by the similar attenuation of cytosolic Ca^{2+} concentration rise when either $TRPC4^{-/-}$ or $TRPC(1–7)^{-/-}$ BMSMCs were induced to form osteoclast-like cells in the presence of RANKL, TNFα, or LTB4. Notably, although increased TRAP activity was observed in $TRPC^{-/-}$ osteoclast-like cells, they did not develop the ability to resorb matrix; this is distinct from $Orai1^{-/-}$ osteoclasts that did retain limited ability to resorb matrix (*6*, *7*). Moreover, ELP-004 had no effect on any measured feature of osteoclastogenesis when added to $TRPC4^{-/-}$ or $TRPC(1–7)^{-/-}$ BMSMCs. This suggests that the inhibitory effect of ELP-004 on osteoclastogenesis is entirely dependent on the presence of functional TRPC4. Considered collectively, these data are consistent with BOTH SOCE and TRPC-mediated Ca^{2+} entry contributing to osteoclastogenesis, with the extent of their involvement exhibiting dependence on the presence or absence of proinflammatory cytokines. However, it is important to recognize that TRPC channels are nonselective cation channels. Hence, we cannot rule out the possibility that TRPC channels primarily depolarize the PM, leading to secondary activation of other channels. That said, because Orai1 is NOT activated by depolarization, the loss of membrane potential ultimately decreases Ca^{2+} flux through Orai channels due to decreased driving force. Hence, it is unlikely that TRPC channel activation would stimulation Orai channel activation.

The ability of ELP-004 to inhibit bone erosion in vivo was assessed in a mouse model of RA that mimics human disease (*47*) using a lipid-based nanoemulsion of an ELP-004. The SKG model is ideal for our studies as it produces chronic and progressive polyarthritis for at least 16 weeks when arthritis is induced using zymosan A (*80*) allowing for long-term treatment with ELP-004. In this model, disease is more robust in female mice, which is consistent with human populations where, in the United States, women are twice as likely to develop arthritis than men (*81*). In addition, the most common presentation of RA in humans is inflammatory arthritis involving the small joints of the hands including the metacarpophalangeal, proximal interphalangeal, and wrist joints (*82*). While we scanned the hind paw, joint swellings quantified in the arthritic indices were visible in the front paws of the SKG mice as well; therefore, the SKG model mimics the presentation of human disease.

In previous studies, we presented a comprehensive characterization of ELP-004 pharmacokinetics, genotoxic and off-target effects, and metabolism (*29*). Here, we demonstrated that the small molecule, ELP-004, is safe for long-term, daily administration with no overt toxicities. Current treatments for RA symptoms, such as pain and swelling, include anti-inflammatories (corticosteroids), antimetabolites (methotrexate), nonsteroidal anti-inflammatory drugs (ibuprofen), and biologic disease modifying anti-rheumatic drugs (bDMARDs; TNFα and RANKL inhibitors). These treatments have significant toxicities and often do not prevent bone erosion in patients with RA (*2*). Clinically approved treatments for bone erosion currently include TNF-inhibiting (infliximab, adalimumab, golimumab, certolizumab pegol, and etanercept) and RANKL-inhibiting (denosumab) bDMARDs and the humanized anti-human interleukin-6 receptor antibody, tocilizumab (*83*, *84*). Studies have shown that targeted synthetic DMARDs, such as Janus kinase (JAK) inhibitors, also reduce bone loss in patients (*84*). However, many patients fail these treatments. Therefore, there is substantial need for treatment options that have a different mode of action and fewer side effects in the patient.

The current study suggests that ELP-004 is a potential therapeutic option for the treatment of RA-associated bone erosions. Our data demonstrate significant, albeit small, improvement in bone parameters following treatment, suggesting that further optimization of the delivery system may be necessary to observe maximal reduction of RA-associated bone erosions. Because of differences in measuring techniques often used in human patients as compared to mouse experiments, it is difficult to predict what percentage of improvement in bone parameters would correlate with reduced pain in humans. However, we demonstrate clear differences in visual erosions in the female paws, which is quantified in the cumulative score (Fig. 6F). Furthermore, these data are consistent with human clinical data demonstrating that bone erosions develop early in disease development and that treatment with DMARDs achieves clinical remission or low disease activity primarily by halting the erosive process and may lead to partial repair of bone erosions [reviewed in (*50*)]. Notably, the female femurs also showed an increase in mean BMD from 0.1127 g/cm^3 in vehicle-treated mice to 0.1436 g/cm^3 in ELP-004–treated mice (Fig. 7B) corresponding to a 24% improvement in BMD. Whereas a majority of the studies evaluating the associations between currently available biologics to treat RA and BMD have shown stabilization or slight improvement in BMD (*85*), ELP-004 demonstrates a significant improvement in this parameter. Furthermore, we demonstrate that it is safe for long-term treatment and effective in a simple oral formulation, which would improve patient compliance over an injection or infusion. ELP-004 is also cheap to manufacture and therefore would likely be assessable to a wider range of patients than more expensive drugs currently on the market. As previously noted, patients are likely to report joint pain consistent with arthritis to their general physicians before being referred to a rheumatologist providing opportunities for immediate and early treatment with a daily capsule of ELP-004.

We were intrigued and surprised to find an interspecies difference in TRPC expression in osteoclasts between mouse and human. Although each TRPC channel has unique properties, all seven TRPC channels are nonselective cation channels activated downstream of PLC. Hence, TRPC channels are fully capable of partially compensating for each other, a concept that has been observed in

knockout models, with physiological implications (*86*). While that did not occur in TRPC4$^{-/-}$ BMSMCs, the fact that human osteoclasts use a different TRPC family member than murine osteoclasts is consistent with their partial redundancy. The extent to which their unique properties differentially support osteoclastogenesis in human versus mouse has not been determined, although future investigations introducing TRPC1 into TRPC4$^{-/-}$ murine cells and/or introducing TRPC4 into TRPC1$^{-/-}$ human cells could provide insight into this intriguing question.

Within the current investigation, we have revealed a previously unidentified role for TRPC-mediated Ca^{2+} entry and osteoclastogenesis driven by the inflammatory cytokines TNFα and LTB4. Furthermore, we have established that the 3,4-dichloropropionanilide analog, ELP-004, is primarily a TRPC channel inhibitor that selectively inhibits the maturation and multinucleation of osteoclasts stimulated by inflammatory cytokines, TNFα and LTB4, with relatively modest effects on physiological osteoclastogenesis (controlled by RANKL alone). We hypothesize that this difference reflects a greater role for TRPC channel–mediated Ca^{2+} elevation in pathological osteoclastogenesis. Given its exceptional safety profile (*29*) and efficacy protecting against bone erosion in vivo shown here, these studies provide a previously unknown mechanism for protection by ELP-004 and reveal fundamental differences between physiological and pathological osteoclastogenesis. Moreover, given the specific effect of ELP-004 on pathophysiological osteoclastogenesis in both murine and human samples, these investigations provide proof of principle for its potential use as a therapeutic for the treatment of arthritis-induced bone erosion.

MATERIALS AND METHODS

Materials

Recombinant mouse mCSF was purchased from R&D Systems Inc (Bio-Techne, Minneapolis) and used at a concentration of 50 ng/ml. Recombinant human mCSF was purchased from MP Biomedicals (California) and used at a concentration of 50 ng/ml. Recombinant solution of receptor activator of NF-κB Ligand (RANKL) was also purchased from R&D Systems Inc, mouse TNFα was purchased from Invitrogen (Waltham, MA), and LB4 was purchased from Cayman Chemicals (Ann Arbor, MI). Recombinant human RANKL and human TNFα were purchased from Enzo Lifesciences (New York). ELP-004 was provided by J. Barnett (ExesaLibero Pharma). Two batches were provided to us for use [batch ET190701-2-PID, >99% pure (produced by WuXi AppTec) and another batch produced by Anthem]. TRPC4-GFP and TRPC5-GFP plasmids were created as described previously (*87*). TRPC7-GFP was obtained from Sino Biological.

Ex vivo experiments

TRPC4$^{-/-}$ mice in C57BL/6 background (*88*) were generously provided by M. Freichel (Heidelberg University) and housed in the animal facility of the University of Texas Health Science Center at Houston, with free access to food and water under controlled light and temperature conditions. Animal experiments were approved by the UT Houston Institutional Animal Care and Use Committee (protocol AWC-22-0030). At 6 weeks old, mice were anesthetized by isoflurane before they were euthanized following procedures in accordance with NIH guidelines and approved by the Animal Welfare Committee of the University of Texas Health Science Center at Houston. TRPC(1–7) HeptaKO [TRPC(1–7)$^{-/-}$] mice in mixed background (*89*) were generously provided by L. Birnbaumer (National Institute of Environmental Health Sciences) and housed in the animal facility of the Medical University of Graz, with free access to food and water under controlled light and temperature conditions. TRPC(1–7)$^{-/-}$ mice and aged-matched outbred wild-type controls were anesthetized by isoflurane before they were euthanized following procedures in accordance with NIH guidelines and approved by the Animal Welfare Committee of the Medical University of Graz. Spleens and bone marrow were dissected and shipped to West Virginia University for further experimentation.

Cell culture

HEK293 cells were cultured using Dulbecco's modified Eagle's medium (DMEM) supplemented with 10% fetal bovine serum and antibiotics [gentamicin (25 μg/ml), fungin (10 μg/ml), and plasmocin (5 μg/ml)]. TRPC3 and TRPC6 stably expressing HEK293 cells were generously provided by Y. Zhou and D. L. Gill (Penn State University). Human EDTA-treated blood samples were provided to us by Dr. G. S. Gerhard (Temple University). TRPC3-expressing cells were maintained in DMEM as above supplemented with geneticin (200 μg/ml) as a selection marker. TRPC6-expressing cells were maintained in DMEM as above supplemented with hygromycin B (100 ng/ml) as a selection marker. In addition, because TRPC6 expression was under the control of an inducible promoter, TRPC6 expression was induced by adding 1 μM ponasterone A 48 hours before experiments. Murine monocyte cells were isolated from bone marrow and spleen (BMSMCs) freshly isolated from C57Bl/6 mice, TRPC4$^{-/-}$ mice, and TRPC(1–7)$^{-/-}$ mice and cultured in α–minimum essential medium (Gibco, Waltham, MA) supplemented with 10% fetal bovine serum, mCSF (50 ng/ml) and antibiotics [gentamicin (25 μg/ml), 1× fungin, and 1× plasmocin]. After 24 hours, they were treated with RANKL (either 1 ng/ml or 100 ng/ml) as per experimental conditions. After 2 to 3 days in culture with RANKL, cells were further treated with TNFα (2 ng/ml) (*31*), 50 nM LTB4, and 100 nM ELP-004 where indicated. Murine osteoclast cultures were maintained for a period of 14 to 21 days as specified in the results and were supplemented with fresh media and treatments every 3 to 5 days. Human PBMCs were extracted from blood samples as previously reported (*56*, *90*) and cultured in α–minimum essential medium supplemented with 10% fetal bovine serum, human mCSF (50 ng/ml), and antibiotics [gentamicin (25 μg/ml), 1× fungin, and 1× plasmocin]. After 24 hours, they were treated with human RANKL (either 1 ng/ml or 100 ng/ml) as per experimental conditions. After 2 to 3 days in culture with RANKL, cells were further treated with human TNFα (2 ng/ml) and 100 nM ELP-004 where indicated.

Electroporation

HEK293 cells (1×10^6) were resuspended in 800 μl of Opti-MEM and transiently transfected via electroporation. Two hours after transfection, cells were supplemented with 10% fetal bovine serum and gentamicin (25 μg/ml). After 24 hours, transfected cells were plated in complete DMEM and cultured for 48 hours in normal conditions with selection markers. Cells expressing high GFP signal were considered successfully transfected and were analyzed.

Generating stable cell lines

HEK293 cells were transfected with STIM1–yellow fluorescent protein (YFP) and STIM2-YFP via electroporation. Cells were grown under normal conditions for 3 days after transfection before selection by puromycin (5 μg/ml). Single-clone colonies expressing the highest amount of YFP were used to generate a stable cell line. Following that, STIM1 and STIM2 stable cells were transfected with Orai 1–cyan fluorescent protein (CFP), Orai 2-CFP, and Orai 3-CFP via electroporation, grown for 3 days under normal condition before selection with G418 and single-clone generation. Clones with the highest YFP and CFP fluorescence intensity were expanded and further screened for SOCE on a Leica DM1 6000B fluorescence microscope controlled by Slidebook software. A single colony was selected for each cell type as specified in the results and expanded for use.

Cytosolic Ca^{2+} and Sr^{2+} measurement

Cells grown on coverslips for 1, 7, 14, and 21 were incubated in a cation-safe buffer [107 mM NaCl, 7.2 mM KCl, 1.2 mM $MgCl_2$, 11.5 mM D-glucose, 20 mM Hepes-NaOH, and 1 mM $CaCl_2$ (pH 7.2)] and loaded with Fura2-acetoxymethyl ester [2 μM; 30 min, room temperature (RT)] as previously described (*5*, *91*). After that, cells were washed in the cation-safe buffer and allowed to de-esterify for 30 min. Following that, cells were treated with 2 μM thapsigargin, a SERCA inhibitor, and varying concentrations of ELP-004 for 10 min in a nominally Ca^{2+}-free solution [107 mM NaCl, 7.2 mM KCl, 1.2 mM $MgCl_2$, 11.5 mM D-glucose, 20 mM Hepes-NaOH, and 0 mM $CaCl_2$ (pH 7.2)] before imaging to deplete the ER Ca^{2+} content of the cells. Fluorescent measurements were made using a Leica DMI 6000B fluorescence microscope controlled by Slidebook Software (Intelligent Imaging Innovations, Denver, CO). After obtaining a stable baseline, 1 mM Ca^{2+} or 3 mM Sr^{2+} was added to the extracellular solution, and SOCE, basal Ca^{2+} concentration, or TRPC channel-mediated Sr^{2+} entry was measured as previously described (*91*). Cytosolic Ca^{2+} or Sr^{2+} levels are presented as ratios of 340/380 nm.

Electrophysiology

Whole-cell voltage-clamp recordings were performed using a voltage ramp protocol (from −100 to +100 mV within 200 ms, with an interval of 5 s between sweeps) on HEK293 cells that transiently expressed mouse TRPC4β as previously described (*92*). Cells were placed in the normal bath solution containing 140 mM NaCl, 5 mM KCl, 2 mM $CalCl_2$, 1 mM $MgCl_2$, 10 mM Hepes, and 10 mM glucose (pH 7.4) and accessed with a patch pipette filled with 110 mM CsCl, 6.6 mM $CaCl_2$, 10 mM 1,2-bis(2-aminophenoxy)ethane-*N*,*N*,*N*′,*N*′-tetraacetic acid (free $[Ca^{2+}] = 400$ nM), and 10 mM Hepes (pH 7.2) to establish the whole-cell configuration. Voltage ramps were applied repeatedly from the holding potential of 0 mV. After establishing the baseline current (~30 s), a nominally Ca^{2+} free bath solution containing 140 mM NaCl, 5 mM KCl, 1 mM $MgCl_2$, 10 mM Hepes, and 10 mM glucose (pH 7.4) was applied through a gravity-driven, multichannel perfusion device, with the outlet positioned ~100 μm away from the cell. EA (30 nM) and ELP-004 (10, 30, 100, and 1000 nM) were diluted to the normally Ca^{2+}-free bath solution at desired final concentrations. EA was applied at ~30 s after the application of the normally Ca^{2+}-free bath solution; EA plus ELP-004 was applied ~10 s after the EA-evoked currents reached the peak and continued for ~90 to 100 s. Then, the drugs were washed with the normally Ca^{2+}-free bath solution. For quantification, the current density at +100 mV and − 100 mV at 45 s after the addition of EA plus ELP-004 were normalized to that at the peak.

Fluorescent TRAP staining

Mouse BMSMC- and human PBMC-derived osteoclasts were grown on 12-mm coverslips for up to 21 and 14 days, respectively, supplemented as per the conditions described in results and stained for tartrate-resistant acid phosphatase using ELF-97 substrate (Invitrogen, catalog no. E6588). At the indicated time points (1, 7, 14, and 21 days for murine osteoclasts and 14 days for human osteoclasts), cells were fixed [2% paraformaldehyde in phosphate-buffered saline (PBS); 30 min, RT]. The tartrate buffer was made as previously described (*93*) (110 mM acetate, 1.1 mM sodium nitrite, and 7.4 mM tartrate), with the additional 200 μM ELF-97 substrate. Cells were incubated in this solution for 15 min at room temperature. Following this, cells were permeabilized (0.1% Triton X-100 in PBS; 1 min, RT) and counterstained for nuclear DNA using 1× 7-AAD (7-aminoactinomycin D; 1:1000 in PBS; 20 min, RT). Cells were visualized by confocal microscopy (Leica SP8 Laser Scanning Microscope). ELF-97 signal was visualized using the 4′,6-diamidino-2-phenylindole longpass filter set, which provides the required ultraviolet (UV) excitation and transmits wavelengths more than 400 nm. Cells were analyzed for TRAP signal intensity, number of TRAP-positive cells per field, and number of nuclei per cell to account for multinucleation.

Immunofluorescence probing for NFATc1

Mouse BMSMC-derived osteoclast-like cells were grown on 12-mm coverslips for 24 hours, 7 days, 14 days, and 21 days. At each of the time points, cells were fixed (3.7% paraformaldehyde in PBS; 10 min, RT) followed by ice-cold PBS wash. Antigen retrieval was performed by submerging the coverslips in antigen-retrieval buffer [100 mM tris, 5% (w/v) urea (pH 9.5); 95°C, 10 min] followed by PBS washes. Cells were permeabilized [0.2% Tween 20 in PBS (PBST); 10 min, RT] and blocked [1% bovine serum albumin (BSA) and glycine (22.52 mg/ml) in PBST; 30 min, RT]. Cells were incubated in mouse monoclonal NFATc1 antibody (200 ng/ml; clone 7A6; Santa Cruz Biotechnology) (200 ng/ml in PBST with 1% BSA; overnight; 4°C). Secondary antibody staining was done using Alexa Fluor 488 antibody (2 μg/ml; 1 hour, RT). Cells were counterstained using 7-AAD (1:1000 in PBS; 15 to 20 min; RT) were visualized via confocal microscopy. NFATc1 signal was visualized using the UV filter set at 488 nm, and NFATc1 colocalization to the nucleus was analyzed using the Leica LASX software.

Reverse transcription qPCR

Mouse BMSMC-and human PBMC-derived osteoclasts were grown under experimental conditions for up to 14 days and collected as cell pellets. RNA was extracted using a kit (Ambion, Austin, TX), and 250 ng of RNA was converted to cDNA using ezDNAse and the Superscript IV Reverse Transcriptase Assay Kit (Invitrogen) as described (*91*). cDNA was diluted 1:10 for a final working concentration of 25 ng per reaction. Housekeeping 18*S* ribosomal RNA (18*S*) was used as a control, and other genes of interest were amplified using 500 nM mouse-specific (table S3) or human-specific (table S4) primers. Each reaction was mixed with Powerhouse SYBR green (Applied Biosystems, Bedford, MA) and analyzed using QuantStudio8 software (Applied Biosystems).

Pit assay

Mouse BMSMC-derived osteoclast-like cells were grown under experimental conditions for 7, 14, and 21 days in osteo-assay surface 24-well plates (Corning, catalog no. CLS3987) which are coated with a proprietary synthetic inorganic bone mimetic. Osteoclasts were supplemented with new media every 3 to 5 days. On the day of the assay, medium was aspirated, wells were washed with 1× DPBS, cells were removed using 10% bleach for 5 min, and the matrix was coated with 1% silver nitrate solution. Plates were incubated with exposure to UV light for 20 to 45 min, or until dark precipitate was visible. Plates were washed with diH_2O, coated with 2.5% sodium thiosulphate solution, and dehydrated with 100% ethanol. Pits were visualized at ×20 magnification on EVOS microscope.

Arthritis animal experiments

ELP-004 (ABP-9927, batch A012104089) was synthesized commercially by Anthem Biosciences Pvt. Ltd. (Karnataka, India). ELP-004 stability was monitored using nuclear magnetic resonance and high-performance liquid chromatography by Anthem Biosciences every 6 months for a total of 2 years; the compound was >97.5% pure (table S1). ELP-004 was formulated into lipid nanoparticle (1 mg/ml; ELP-004–NP) and lipid nanoemulsion (30 mg/ml; ELP-004–LNE) solutions for daily administration by intraperitoneal or oral gavage, respectively. See Supplementary Methods for details.

Animal experiments were conducted at West Virginia University (WVU) and approved by the WVU Institutional Animal Care and Use Committee (protocol 1604002075). SKG breeding pairs were a generous gift from H. Rosenzweig at Oregon Health and Science (with permission from S. Sakaguchi). An SKG breeding colony was maintained at WVU to produce aged-matched cohorts for experiments. All mice were housed in a specific pathogen–free (SPF) barrier facility with 12-hour light/12-hour dark cycles and fed normal chow.

Raised under SPF conditions, SKG animals do not spontaneously develop RA. RA was induced in the male and female SKG mice at 8 weeks of age by a single intraperitoneal injection of 2 mg of zymosan A (Z4250, Sigma-Aldrich, St Louis MO) in sterile saline. Each paw was scored by a treatment-blinded observer as described (*48*) for arthritis weekly until day 56. Briefly, an arthritic index (AI) was determined by scoring each paw individually on a scale of 0 to 4: 0, normal; 1, mild, but definite redness and swelling limited to individual digits; 2, two swollen joints/digits; 3, three or more swollen joints/digits; 4, severe swelling of all joints/digits. All paws were evaluated; maximal AI per mouse was 16. To minimize the need to bear weight on the hind paws, arthritic mice were given moist chow on the cage floor. Mice with severe arthritis were given soft bedding to lessen the pain associated with mobility.

On day 56, mice were euthanized. Blood was collected via cardiac puncture. Plasma was isolated for cytokine analysis. The left rear leg and paw as well as the spine were fixed in 10% formalin for 3D evaluation for bone erosion using μCT. Right paws were fixed in 10% formalin for histology. Bone marrow was isolated from the rear right femur and tibia.

MicroCT

μCT was performed on a SkyScan 1272 (Bruker, Billerica MA). Images were processed and analyzed by Bruker software (*94*). Briefly, the left rear limbs of each animal were scanned in 70% ethanol using the following parameters: isometric voxel size of 7 μm (5 μm for spines), tube voltage (x-ray tube potential) of 60 kV, tube current of 166 μA, exposure time of 650 ms, and aluminum filter of 0.25 mm. The cross-section images were reconstructed using NRecon (version 1.7.1.0, Bruker) with a 20% correction to reduce beam hardening and ring artifacts applied where appropriate. Bones were analyzed with DataViewer (Bruker) and CTAn (version 1.16.9.0+, Bruker), and images were prepared in CTVox (version 3.3.0r1403, Bruker). The tarsus region of interest (ROI) was selected from the distal tibia to the proximal metatarsal bones. For the calcaneus, 1.41 mm (201 slices) was analyzed beginning at the tip. 3D analysis was performed after anisotropic diffusion filtering, global thresholding (min = 100), and ROI Shrink-Wrap (mode: shrink wrap, 3D space, stretch over holes, diameter of 50 voxels), closure (radius of 4), and erosion (radius of 1) to measure porosity (%; volume of pores/volume of interest). The image was inverted to quantify the connectivity density (1/mm^3) of the pores. For trabecular bone in the femurs, the distal epiphysis (growth plate) was used as a reference point, and the ROI was offset proximal to ensure that no growth plate was included in the analysis. A total of 1.75 mm (250 slices) or 2.15 mm (430 slices) was analyzed for the femur and L5 spine, respectively. Trabeculae were delineated from cortical bone using a manual assessment every 15 to 20 slices. Bone mineral density (BMD) was calculated after calibration with calcium hydroxyapatite phantoms of known density: 0.25 and 0.75 g/cm^3. Images of representative mice of each group are presented.

Metatarsal scoring

The metatarsals for digits 2 to 5 were scored visually in each mouse by an observer blinded to the treatment, as previously described (*95*). Briefly, each digit was scored on a scale of 0 to 3: 0, normal, no signs of erosion; 1, roughness of bone surface; 2, pitting/indentations; and 3, full thickness holes. Cumulative scores (max = 12) for each mouse were compared between groups with one-way or unpaired *t* test.

Statement about statistical tests

All statistical analyses were done using suggested analyses by GraphPad Prism software.

Statement about data inclusion

Any excluded data was based on human error that met pre-established criteria including correct handling of reagents, correct administration of treatments to cells, proper animal handling and dissection, and proper rigor and reproducibility of results.

Supplementary Materials

This PDF file includes:

Supplementary Methods
Figs. S1 to S23
Tables S1 to S4

REFERENCES AND NOTES

1. S. H. Till, M. L. Snaith, Assessment, investigation, and management of acute monoarthritis. *J. Accid. Emerg. Med.* **16**, 355–361 (1999).
2. R. Costello, T. David, M. Jani, Impact of adverse events associated with medications in the treatment and prevention of rheumatoid arthritis. *Clin. Ther.* **41**, 1376–1396 (2019).
3. K. Jung Ha, K. Nacksung, Signaling pathways in osteoclast differentiation. *Chonnam Med. J.* **52**, 12–17 (2016).

4. T. Suda, N. Takahashi, N. Udagawa, E. Jimi, M. T. Gillespie, T. J. Martin, Modulation of osteoclast differentiation and function by the new members of the tumor necrosis factor receptor and ligand families. *Endocr. Rev.* **20**, 345–357 (1999).
5. Y. Zhou, T. L. Lewis, L. J. Robinson, K. M. Brundage, R. Schafer, K. H. Martin, H. C. Blair, J. Soboloff, J. B. Barnett, The role of calcium release activated calcium channels in osteoclast differentiation. *J. Cell. Physiol.* **226**, 1082–1089 (2011).
6. L. J. Robinson, S. Mancarella, D. Songsawad, I. L. Tourkova, J. B. Barnett, D. L. Gill, J. Soboloff, H. C. Blair, Gene disruption of the calcium channel Orai1 results in inhibition of osteoclast and osteoblast differentiation and impairs skeletal development. *Lab. Invest.* **92**, 1071–1083 (2012).
7. L. J. Robinson, J. Soboloff, I. L. Tourkova, Q. C. Larrouture, M. R. Witt, S. Gross, R. Hooper, E. Samakai, P. F. Worley, J. B. Barnett, H. C. Blair, The function of the calcium channel Orai1 in osteoclast development. *FASEB J* **35**, e21653 (2021).
8. C. Tetta, G. Camussi, V. Modena, C. D. Vittorio, C. Baglioni, Tumour necrosis factor in serum and synovial fluid of patients with active and severe rheumatoid arthritis. *Ann. Rheum. Dis.* **49**, 665–667 (1990).
9. T. Yamashita, Z. Yao, F. Li, Q. Zhang, I. R. Badell, E. M. Schwarz, S. Takeshita, E. F. Wagner, M. Noda, K. Matsuo, L. Xing, B. F. Boyce, NF-κB p50 and p52 regulate receptor activator of NF-κB ligand (RANKL) and tumor necrosis factor-induced osteoclast precursor differentiation by activating c-Fos and NFATc1. *J. Biol. Chem.* **282**, 18245–18253 (2007).
10. L.-X. Zheng, K.-X. Li, S.-L. Yang, Pain and bone damage in rheumatoid arthritis: Role of leukotriene B4. *Clin. Exp. Rheumatol.* **37**, 872–878 (2019).
11. H.-C. Lin, T.-H. Lin, M.-Y. Wu, Y.-C. Chiu, C.-H. Tang, M.-J. Hour, H.-C. Liou, H.-J. Tu, R.-S. Yang, W.-M. Fu, 5-Lipoxygenase inhibitors attenuate TNF-α-induced inflammation in human synovial fibroblasts. *PLOS ONE* **9**, e107890 (2014).
12. J. S. Bomalaski, M. A. Clark, Phospholipase A_2 and arthritis. *Arthritis Rheum.* **36**, 190–198 (1993).
13. J. Martel-Pelletier, D. Lajeunesse, P. Reboul, J.-P. Pelletier, Therapeutic role of dual inhibitors of 5-LOX and COX, selective and non-selective non-steroidal anti-inflammatory drugs. *Ann. Rheum. Dis.* **62**, 501–509 (2003).
14. T. Gürsel, S. Firat, Z. S. Ercan, Increased serum leukotriene B4 level in the active stage of rheumatoid arthritis in children. *Prostaglandins Leukot. Essent. Fatty Acids* **56**, 205–207 (1997).
15. H. C. Blair, P. H. Schlesinger, C. L. Huang, M. Zaidi, Calcium signalling and calcium transport in bone disease. *Subcell Biochem.* **45**, 539–562 (2007).
16. D. E. Clapham, L. W. Runnels, C. Strübing, The trp ion channel family. *Nat. Rev. Neurosci.* **2**, 387–396 (2001).
17. C. B. Klee, H. Ren, X. Wang, Regulation of the calmodulin-stimulated protein phosphatase, calcineurin. *J. Biol. Chem.* **273**, 13367–13370 (1998).
18. K. Sato, A. Suematsu, T. Nakashima, S. Takemoto-Kimura, K. Aoki, Y. Morishita, H. Asahara, K. Ohya, A. Yamaguchi, T. Takai, T. Kodama, T. A. Chatila, H. Bito, H. Takayanagi, Regulation of osteoclast differentiation and function by the CaMK-CREB pathway. *Nat. Med.* **12**, 1410–1416 (2006).
19. L. P. He, T. Hewavitharana, J. Soboloff, M. A. Spassova, D. L. Gill, A functional link between store-operated and TRPC channels revealed by the 3,5-bis(trifluoromethyl)pyrazole derivative, BTP2. *J. Biol. Chem.* **280**, 10997–11006 (2005).
20. H. L. Ong, K. T. Cheng, X. Liu, B. C. Bandyopadhyay, B. C. Paria, J. Soboloff, B. Pani, Y. Gwack, S. Srikanth, B. B. Singh, D. L. Gill, I. S. Ambudkar, Dynamic assembly of TRPC1-STIM1-Orai1 ternary complex is involved in store-operated calcium influx. Evidence for similarities in store-operated and calcium release-activated calcium channel components. *J. Biol. Chem.* **282**, 9105–9116 (2007).
21. J. Soboloff, B. S. Rothberg, M. Madesh, D. L. Gill, STIM proteins: Dynamic calcium signal transducers. *Nat. Rev. Mol. Cell Biol.* **13**, 549–565 (2012).
22. Y. Cai, L. J. Stafford, B. A. Bryan, D. Mitchell, M. Liu, G-protein-activated phospholipase C-β, new partners for cell polarity proteins Par3 and Par6. *Oncogene* **24**, 4293–4300 (2005).
23. J. W. Putney, Physiological mechanisms of TRPC activation. *Pflugers Arch.* **451**, 29–34 (2005).
24. J. Jeon, J. B. Tian, M. X. Zhu, TRPC4 as a coincident detector of G(i/o) and G(q/11) signaling: Mechanisms and pathophysiological implications. *Curr. Opin. Physiol.* **17**, 34–41 (2020).
25. S. Klein, B. Mentrup, M. Timmen, J. Sherwood, O. Lindemann, M. Fobker, D. Kronenberg, T. Pap, M. J. Raschke, R. Stange, Modulation of transient receptor potential channels 3 and 6 regulates osteoclast function with impact on trabecular bone loss. *Calcif. Tissue Int.* **106**, 655–664 (2020).
26. E. C. Ong, V. Nesin, C. L. Long, C. X. Bai, J. L. Guz, I. P. Ivanov, J. Abramowitz, L. Birnbaumer, M. B. Humphrey, L. Tsiokas, A TRPC1 protein-dependent pathway regulates osteoclast formation and function. *J. Biol. Chem.* **288**, 22219–22232 (2013).
27. H. C. Blair, J. Soboloff, L. J. Robinson, I. L. Tourkova, Q. C. Larrouture, M. R. Witt, I. Holaskova, R. Schafer, M. Elliott, R. Hirsch, J. B. Barnett, Suppression of arthritis-induced bone erosion by a CRAC channel antagonist. *RMD Open* **2**, e000093 (2016).
28. T. L. Lewis, "Alterations in T cell function and activation during exposure to the herbicide 3,4 dichloropropionanilide (DCPA) and its metabolites", thesis, West Virginia University, West Virginia, USA (2010).
29. J. L. McCall, W. J. Geldenhuys, L. J. Robinson, M. R. Witt, P. M. Gannett, B. C. G. Soderberg, H. C. Blair, J. Soboloff, J. B. Barnett, Preclinical evaluation of ELP-004 in mice. *Pharmacol. Res. Perspect.* **12**, e1230 (2024).
30. K. Venkatachalam, F. Zheng, D. L. Gill, Regulation of canonical transient receptor potential (TRPC) channel function by diacylglycerol and protein kinase C. *J. Biol. Chem.* **278**, 29031–29040 (2003).
31. J. Lam, S. Takeshita, J. E. Barker, O. Kanagawa, F. P. Ross, S. L. Teitelbaum, TNF-α induces osteoclastogenesis by direct stimulation of macrophages exposed to permissive levels of RANK ligand. *J. Clin. Invest.* **106**, 1481–1488 (2000).
32. G. D. Kalliolias, L. B. Ivashkiv, TNF biology, pathogenic mechanisms and emerging therapeutic strategies. *Nat. Rev. Rheumatol.* **12**, 49–62 (2016).
33. Y. Akbulut, H. J. Gaunt, K. Muraki, M. J. Ludlow, M. S. Amer, A. Bruns, N. S. Vasudev, L. Radtke, M. Willot, S. Hahn, T. Seitz, S. Ziegler, M. Christmann, D. J. Beech, H. Waldmann, (−)-Englerin A is a potent and selective activator of TRPC4 and TRPC5 calcium channels. *Angew. Chem. Int. Ed. Engl.* **54**, 3787–3791 (2015).
34. J. Y. Kang, N. Kang, Y.-M. Yang, J. H. Hong, D. M. Shin, The role of Ca^{2+}-NFATc1 signaling and its modulation on osteoclastogenesis. *INt. J. Mol. Sci.* **21**, 3646 (2020).
35. J. H. Kim, N. Kim, Regulation of NFATc1 in osteoclast differentiation. *J. Bone Metab.* **21**, 233–241 (2014).
36. S. Y. Hwang, J. W. Putney Jr., Calcium signaling in osteoclasts. *Biochim. Biophys. Acta* **1813**, 979–983 (2011).
37. M. Yagi, T. Miyamoto, Y. Sawatani, K. Iwamoto, N. Hosogane, N. Fujita, K. Morita, K. Ninomiya, T. Suzuki, K. Miyamoto, Y. Oike, M. Takeya, Y. Toyama, T., Suda DC-STAMP is essential for cell–cell fusion in osteoclasts and foreign body giant cells. *J. Exp. Med.* **202**, 345–351 (2005).
38. J. Kodama, T. Kaito, Osteoclast multinucleation: review of current literature. *Int. J. Mol. Sci.* **21**, 5685 (2020).
39. Y.-H. Chiu, E. Schwarz, D. Li, Y. Xu, T.-R. Sheu, J. Li, K. L. de Mesy Bentley, C. Feng, B. Wang, J.-C. Wang, L. Albertorio-Saez, R. Wood, M. Kim, W. Wang, C. T. Ritchlin, Dendritic cell-specific transmembrane protein (DC-STAMP) regulates osteoclast differentiation via the Ca^{2+}/NFATc1 axis. *J. Cell. Physiol.* **232**, 2538–2549 (2017).
40. T. L. Lewis, K. M. Brundage, R. A. Brundage, J. B. Barnett, 3,4-Dichloropropionanilide (DCPA) inhibits T-cell activation by altering the intracellular calcium concentration following store depletion. *Toxicol. Sci.* **103**, 97–107 (2008).
41. T. L. Lewis, I. Holaskova, J. B. Barnett, The toxicity of the N-hydroxy and 6-hydroxy metabolites of 3,4-dichloropropionanilide does not depend on calcium release-activated calcium channel inhibition. *Toxicol. Sci.* **131**, 395–405 (2013).
42. J. B. Barnett, J. Gandy, D. Wilbourn, S. A. Theus, Comparison of the immunotoxicity of propanil and its metabolite, 3,4-dichloroaniline, in C57Bl/6 mice. *Fundam. Appl. Toxicol.* **18**, 628–631 (1992).
43. K. M. Brundage, J. B. Barnett, J. E. Mahaney, The amide class herbicide 3,4-dichloropropionanilide (DCPA) alters the mobility of hydrocarbon chains in T-lymphocyte but not macrophage membranes. *J. Toxicol. Environ. Health A* **66**, 2253–2265 (2003).
44. D. C. McMillan, J. E. Leakey, M. P. Arlotto, J. M. McMillan, J. A. Hinson, Metabolism of the arylamide herbicide propanil. II. Effects of propanil and its derivatives on hepatic microsomal drug-metabolizing enzymes in the rat. *Toxicol. Appl. Pharmacol.* **103**, 102–112 (1990).
45. P. Saralkar, T. Arsiwala, W. J. Geldenhuys, Nanoparticle formulation and in vitro efficacy testing of the mitoNEET ligand NL-1 for drug delivery in a brain endothelial model of ischemic reperfusion-injury. *Int. J. Pharm.* **578**, 119090 (2020).
46. N. Sakaguchi, T. Takahashi, H. Hata, T. Nomura, T. Tagami, S. Yamazaki, T. Sakihama, T. Matsutani, I. Negishi, S. Nakatsuru, S. Sakaguchi, Altered thymic T-cell selection due to a mutation of the ZAP-70 gene causes autoimmune arthritis in mice. *Nature* **426**, 454–460 (2003).
47. S. Tanaka, S. Maeda, M. Hashimoto, C. Fujimori, Y. Ito, S. Teradaira, K. Hirota, H. Yoshitomi, T. Katakai, A. Shimizu, T. Nomura, N. Sakaguchi, S. Sakaguchi, Graded attenuation of TCR signaling elicits distinct autoimmune diseases by altering thymic T cell selection and regulatory T cell function. *J. Immunol.* **185**, 2295–2305 (2010).
48. J. L. McCall, H. C. Blair, K. E. Blethen, C. Hall, M. Elliott, J. B. Barnett, Prenatal cadmium exposure does not induce greater incidence or earlier onset of autoimmunity in the offspring. *PLOS ONE* **16**, e0249442 (2021).
49. K. K. Keller, L. M. Lindgaard, L. Wogensen, F. Dagnæs-Hansen, J. S. Thomsen, S. Sakaguchi, K. Stengaard-Pedersen, E.-M. Hauge, SKG arthritis as a model for evaluating therapies in rheumatoid arthritis with special focus on bone changes. *Rheumatol. Int.* **33**, 1127–1133 (2013).
50. P. K. Panagopoulos, G. I. Lambrou, Bone erosions in rheumatoid arthritis: Recent developments in pathogenesis and therapeutic implications. *J. Musculoskelet. Neuronal Interact* **18**, 304–319 (2018).

51. L. Quan, Y. Zhang, A. Dusad, K. Ren, P. E. Purdue, S. R. Goldring, D. Wang, The evaluation of the therapeutic efficacy and side effects of a macromolecular dexamethasone prodrug in the collagen-induced arthritis mouse model. *Pharm. Res.* **33**, 186–193 (2016).
52. S. Seeuws, P. Jacques, J. Van Praet, M. Drennan, J. Coudenys, T. Decruy, E. Deschepper, L. Lepescheux, P. Pujuguet, L. Oste, N. Vandeghinste, R. Brys, G. Verbruggen, D. Elewaut, A multiparameter approach to monitor disease activity in collagen-induced arthritis. *Arthritis Res. Ther.* **12**, R160 (2010).
53. S. Moshayedi, B. Tasorian, A. Almasi-Hashiani, The prevalence of osteoporosis in rheumatoid arthritis patient: A systematic review and meta-analysis. *Sci. Rep.* **12**, 15844 (2022).
54. P. Fardellone, E. Salawati, L. Le Monnier, V. Goeb, Bone loss, osteoporosis, and fractures in patients with rheumatoid arthritis: A review. *J. Clin. Med.* **9**, 3361 (2020).
55. P.-L. Chung, S. Zhou, B. Eslami, L. Shen, M. S. LeBoff, J. Glowacki, Effect of age on regulation of human osteoclast differentiation. *J. Cell. Biochem.* **115**, 1412–1419 (2014).
56. G. Ciapetti, G. Di Pompo, S. Avnet, D. Martini, A. Diez-Escudero, E. B. Montufar, M.-P. Ginebra, N. Baldini, Osteoclast differentiation from human blood precursors on biomimetic calcium-phosphate substrates. *Acta Biomaterialia* **50**, 102–113 (2017).
57. D. Umlauf, H. Hidding, O. Lindemann, B. Dankbar, S. Frank, C. Cromme, A. Dietrich, R. P. Marshall, M. Amling, M. Steiner, U. Kornak, A. Schwab, T. Pap, J. Bertrand, Transient receptor potential canonical channel 1 dependent pathways are required for osteoclast fusion and mediate osteoporotic bone loss. *Ann. Rheum. Dis.* **71**, A67.2–A6A67 (2012).
58. W. Pruzanski, P. Vadas, E. Stefanski, M. B. Urowitz, Phospholipase A2 activity in sera and synovial fluids in rheumatoid arthritis and osteoarthritis. Its possible role as a proinflammatory enzyme. *J. Rheumatol.* **12**, 211–216 (1985).
59. M. Feldman, I. Ginsburg, A novel hypothetical approach to explain the mechanisms of pathogenicity of rheumatic arthritis. *Mediterr. J. Rheumatol.* **32**, 112–117 (2021).
60. R. Liu, Y. Chen, W. Fu, S. Wang, Y. Cui, X. Zhao, Z.-N. Lei, A. Hettinghouse, J. Liu, C. Wang, C. Zhang, Y. Bi, G. Xiao, Z.-S. Chen, C.-j. Liu, Fexofenadine inhibits TNF signaling through targeting to cytosolic phospholipase A2 and is therapeutic against inflammatory arthritis. *Ann. Rheum. Dis.* **78**, 1524–1535 (2019).
61. L. Xia, D. Zhang, C. Wang, F. Wei, Y. Hu, PC-PLC is involved in osteoclastogenesis induced by TNF-α through upregulating IP3R1 expression. *FEBS Lett.* **586**, 3341–3348 (2012).
62. K. Kobayashi, N. Takahashi, E. Jimi, N. Udagawa, M. Takami, S. Kotake, N. Nakagawa, M. Kinosaki, K. Yamaguchi, N. Shima, H. Yasuda, T. Morinaga, K. Higashio, T. J. Martin, T. Suda, Tumor necrosis factor alpha stimulates osteoclast differentiation by a mechanism independent of the ODF/RANKL-RANK interaction. *J. Exp. Med.* **191**, 275–286 (2000).
63. Y. Takayama, S. Derouiche, K. Maruyama, M. Tominaga, Emerging perspectives on pain management by modulation of TRP Channels and ANO1. *Int. J. Mol. Sci.* **20**, 3411 (2019).
64. K. Kobayashi, N. Takahashi, E. Jimi, N. Udagawa, M. Takami, S. Kotake, N. Nakagawa, M. Kinosaki, K. Yamaguchi, N. Shima, H. Yasuda, T. Morinaga, K. Higashio, T. J. Martin, T. Suda, Tumor necrosis factor α stimulates osteoclast differentiation by a mechanism independent of the Odf/Rankl–rank interaction. *J. Exp. Med.* **191**, 275–286 (2000).
65. K. Inoue, C. Ng, Y. Xia, B. Zhao, Regulation of osteoclastogenesis and bone resorption by miRNAs. *Front. Cell. Dev. Biol.* **9**, 651161 (2021).
66. C. Magnusson, D. L. Vaux, Signalling by CD95 and TNF receptors: Not only life and death. *Immunol. Cell. Biol.* **77**, 41–46 (1999).
67. L. J. Robinson, H. C. Blair, J. B. Barnett, J. Soboloff, The roles of Orai and Stim in bone health and disease. *Cell Calcium* **81**, 51–58 (2019).
68. J. Ma, L. Zhu, Z. Zhou, T. Song, L. Yang, X. Yan, A. Chen, T. W. Ye, The calcium channel TRPV6 is a novel regulator of RANKL-induced osteoclastic differentiation and bone absorption activity through the IGF–PI3K–AKT pathway. *Cell Prolif.* **54**, e12955 (2021).
69. M. S. Kim, Y.-M. Yang, A. Son, Y. S. Tian, S.-I. Lee, S. W. Kang, S. Muallem, D. M. Shin, RANKL-mediated reactive oxygen species pathway that induces long lasting Ca^{2+} oscillations essential for osteoclastogenesis. *J. Biol. Chem.* **285**, 6913–6921 (2010).
70. H. Takayanagi, S. Kim, T. Koga, H. Nishina, M. Isshiki, H. Yoshida, A. Saiura, M. Isobe, T. Yokochi, J.-i. Inoue, E. F. Wagner, T. W. Mak, T. Kodama, T. Taniguchi, Induction and activation of the transcription factor NFATc1 (NFAT2) integrate RANKL signaling in terminal differentiation of osteoclasts. *Dev. Cell* **3**, 889–901 (2002).
71. J. Nieto-Felipe, A. Macias-Diaz, J. Sanchez-Collado, A. Berna-Erro, I. Jardin, G. M. Salido, J. J. Lopez, J. A. Rosado, Role of Orai-family channels in the activation and regulation of transcriptional activity. *J. Cell. Physiol.* **238**, 714–726 (2023).
72. J. Di Capite, S. W. Ng, A. B. Parekh, Decoding of cytoplasmic Ca^{2+} oscillations through the spatial signature drives gene expression. *Curr. Biol.* **19**, 853–858 (2009).
73. K.-i. Otsuguro, J. Tang, Y. Tang, R. Xiao, M. Freichel, V. Tsvilovskyy, S. Ito, V. Flockerzi, M. X. Zhu, A. V. Zholos, Isoform-specific Inhibition of TRPC4 Channel by phosphatidylinositol 4,5-Bisphosphate. *J. Biol. Chem.* **283**, 10026–10036 (2008).
74. M. Trebak, L. Lemonnier, W. I. DeHaven, B. J. Wedel, G. S. Bird, J. W. Putney, Complex functions of phosphatidylinositol 4,5-bisphosphate in regulation of TRPC5 cation channels. *Pflügers Archiv. Euro. J. Physiol.* **457**, 757–769 (2009).
75. N. Dixit, D. J. Wu, Y. H. Belgacem, L. N. Borodinsky, M. E. Gershwin, I. E. Adamopoulos, Leukotriene B4 activates intracellular calcium and augments human osteoclastogenesis. *Arthritis Res. Ther.* **16**, 496 (2014).
76. B. C. Paria, A. B. Malik, A. M. Kwiatek, A. Rahman, M. J. May, S. Ghosh, C. Tiruppathi, Tumor necrosis factor-α induces nuclear factor-κB-dependent TRPC1 expression in endothelial cells. *J. Biol. Chem.* **278**, 37195–37203 (2003).
77. K. E. Mace, M. P. Lussier, G. Boulay, J. L. Terry-Powers, H. Parfrey, A. L. Perraud, D. W. Riches, TRUSS, TNF-R1, and TRPC ion channels synergistically reverse endoplasmic reticulum Ca^{2+} storage reduction in response to m1 muscarinic acetylcholine receptor signaling. *J. Cell. Physiol.* **225**, 444–453 (2010).
78. H. J. Gaunt, N. S. Vasudev, D. J. Beech, Transient receptor potential canonical 4 and 5 proteins as targets in cancer therapeutics. *Eur. Biophys. J.* **45**, 611–620 (2016).
79. M. Freichel, R. Vennekens, J. Olausson, M. Hoffmann, C. Müller, S. Stolz, J. Scheunemann, P. Weißgerber, V. Flockerzi, Functional role of TRPC proteins in vivo: Lessons from TRPC-deficient mouse models. *Biochem. Biophys. Res. Commun.* **322**, 1352–1358 (2004).
80. E. J. Lee, E. E. Vance, B. R. Brown, P. S. Snow, J. S. Clowers, S. Sakaguchi, H. L. Rosenzweig, Investigation of the relationship between the onset of arthritis and uveitis in genetically predisposed SKG mice. *Arthritis Res. Ther.* **17**, 218 (2015).
81. C. S. Crowson, E. L. Matteson, E. Myasoedova, C. J. Michet, F. C. Ernste, K. J. Warrington, J. M. Davis III, G. G. Hunder, T. M. Therneau, S. E. Gabriel, The lifetime risk of adult-onset rheumatoid arthritis and other inflammatory autoimmune rheumatic diseases. *Arthritis Rheum.* **63**, 633–639 (2011).
82. M. RH, B. BS, in *StatPearls [Internet]* (StatPearls Publishing, 2024), vol. 2024.
83. C. A. F. Zerbini, P. Clark, L. Mendez-Sanchez, R. M. R. Pereira, O. D. Messina, C. R. Uña, J. D. Adachi, W. F. Lems, C. Cooper, N. E. Lane, IOF Chronic Inflammation and Bone Structure (CIBS) Working Group, Bone structure working, biologic therapies and bone loss in rheumatoid arthritis. *Osteoporosis Int.* **28**, 429–446 (2017).
84. B. Soós, Á. Szentpétery, H. G. Raterman, W. F. Lems, H. P. Bhattoa, Z. Szekanecz, Effects of targeted therapies on bone in rheumatic and musculoskeletal diseases. *Bat. Rev. Rheum.* **18**, 249–257 (2022).
85. J.-F. Chen, C.-Y. Hsu, S.-F. Yu, C.-H. Ko, W.-C. Chiu, H.-M. Lai, Y.-C. Chen, Y.-J. Su, T.-T. Cheng, The impact of long-term biologics/target therapy on bone mineral density in rheumatoid arthritis: A propensity score-matched analysis. *Rheumatology* **59**, 2471–2480 (2020).
86. A. Dietrich, Y. S. M. Mederos, M. Gollasch, V. Gross, U. Storch, G. Dubrovska, M. Obst, E. Yildirim, B. Salanova, H. Kalwa, K. Essin, O. Pinkenburg, F. C. Luft, T. Gudermann, L. Birnbaumer, Increased vascular smooth muscle contractility in *TRPC6*$^{-/-}$ mice. *Mol. Cell Biol.* **25**, 6980–6989 (2005).
87. J. P. Jeon, D. P. Thakur, J. B. Tian, I. So, M. X. Zhu, Regulator of G-protein signalling and GoLoco proteins suppress TRPC4 channel function via acting at Gαi/o. *Biochem. J.* **473**, 1379–1390 (2016).
88. M. Freichel, S. H. Suh, A. Pfeifer, U. Schweig, C. Trost, P. Weissgerber, M. Biel, S. Philipp, D. Freise, G. Droogmans, F. Hofmann, V. Flockerzi, B. Nilius, Lack of an endothelial store-operated Ca^{2+} current impairs agonist-dependent vasorelaxation in TRP4−/− mice. *Nat. Cell Biol.* **3**, 121–127 (2001).
89. K. Formoso, S. Susperreguy, M. Freichel, L. Birnbaumer, RNA-seq analysis reveals TRPC genes to impact an unexpected number of metabolic and regulatory pathways. *Sci. Rep.* **10**, 7227 (2020).
90. D. Figueroa-Tentori, S. Querol, I. A. Dodi, A. Madrigal, R. Duggleby, High purity and yield of natural Tregs from cord blood using a single step selection method. *J. Immunol. Methods* **339**, 228–235 (2008).
91. S. Gross, R. Hooper, D. Tomar, A. P. Armstead, N. a. Shanas, P. Mallu, H. Joshi, S. Ray, P. L.-G. Chong, I. Astsaturov, J. M. Farma, K. Q. Cai, K. N. Chitrala, J. W. Elrod, M. R. Zaidi, J. Soboloff, Suppression of Ca^{2+} signaling enhances melanoma progression. *EMBO J.* **41**, e110046 (2022).
92. D. P. Thakur, Q. Wang, J. Jeon, J. B. Tian, M. X. Zhu, Intracellular acidification facilitates receptor-operated TRPC4 activation through PLCdelta1 in a Ca^{2+}-dependent manner. *J. Physiol.* **598**, 2651–2667 (2020).
93. L. Filgueira, Fluorescence-based staining for tartrate-resistant acidic phosphatase (TRAP) in osteoclasts combined with other fluorescent dyes and protocols. *J. Histochem. Cytochem.* **52**, 411–414 (2004).
94. P. Salmon, "*Application of Bone Morphometry and Densitometry by X-Ray Micro-CT to Bone Disease Models and Phenotypes*" (Springer, 2020), pp. 49–75.
95. J. M. Brown, E. Ross, G. Desanti, A. Saghir, A. Clark, C. Buckley, A. Filer, A. Naylor, E. Claridge, Detection and characterisation of bone destruction in murine rheumatoid arthritis using statistical shape models. *Med. Image Anal.* **40**, 30–43 (2017).

Acknowledgments: We would like to thank T. McManus for the assistance in acquiring the mass spectrometry data and P. Lockman for the assistance with tissue drug concentration analysis. **Funding:** This work was supported by NIH grants 1R42AR074812 (to J.B.B.), R01AI152506 (to J.S.) and R01AR076146 (to H.C.B.) and the US Department of Veteran's Affairs BX002490-06A1 (to H.C.B.). Imaging experiments and image analysis were performed in the WVU Animal Models & Imaging Facility, which has been supported by the WVU Cancer Institute, the WVU HSC Office of Research and Graduate Education, and NIH grants P20GM121322 and U54GM104942. The WVU Flow Cytometry & Single Cell Core Facility

(RRID:SCR_017738) and equipment used here is supported by NIH grant U51 GM104942 (WV CTSI), by the NIH equipment grant S10OD016165, and by the Institutional Development Awards (IDeA) from the NIGMS P20GM109098 (Stroke CoBRE), P30GM121322 (TME CoBRE), and P20GM103434 (INBRE). Liquid chromatography tandem mass spectrometry analyses were performed in the WVU Metabolomics & Small Molecule Analysis Facility, which has been supported by the WVU Cancer Institute, the WVU HSC Office of Research & Graduate Education, and NIH grant P20GM103434. **Author contributions:** S.R.: Writing—original draft, conceptualization, investigation, writing—review and editing, methodology, data curation, validation, supervision, formal analysis, project administration, and visualization. J.L.M.: Conceptualization, investigation. writing—review and editing, methodology, data curation, validation, supervision, formal analysis, project administration, and visualization. J.B.T.: Investigation, methodology, data curation, validation, and visualization. J.J.: Investigation, resources, and validation, A.D.: Investigation and formal analysis. K.T.: Investigation and validation. S.L.: Investigation and methodology. K.B.: Investigation, data curation, validation, formal analysis, and visualization. B.N.: Conceptualization, investigation, writing–review and editing, methodology, data curation, validation, formal analysis, and visualization. C.H.: Investigation, data curation, validation, formal analysis, and visualization. K.G.: Conceptualization, writing–review and editing, methodology, and resources. B.B.: Investigation, methodology, and resources. W.G.: Conceptualization, investigation, methodology, resources, validation, supervision, formal analysis, and visualization. M.X.Z.: Writing–review and editing, methodology, resources, supervision, and project administration. H.C.B.: Conceptualization, investigation, writing–review and editing, methodology, resources, funding acquisition, validation, supervision, formal analysis, project administration, and visualization. J.B.B.: Conceptualization, writing–review and editing, methodology, resources, funding acquisition, data curation, validation, supervision, and project administration. J.S.: Conceptualization, writing–review and editing, methodology, resources, funding acquisition, data curation, validation, supervision, formal analysis, project administration, and visualization. **Competing interests:** J.B.B. is the President and Chief Scientific Officer of *ExesaLibero* Pharma (*ExesaLibero*); J.S. and H.C.B. are founding members of the Scientific Advisory Board. J.B.B., J.S., and H.C.B. have a patent (US 10,682,320 B2) on methods for inhibiting osteoclast development, which includes the use of ELP-004. J.B.B., J.S., H.C.B., and W.G. have a patent pending (18/336,712) on the mode of action of ELP-004 on TRPC channels. J.L.M., K.B., B.N., and C.H. are current or former employees at ExesaLibero. ExesaLibero is a company that is licensed to commercially develop ELP-004 as a drug to treat bone erosion. 1R42AR074812 was awarded to ExesaLibero. The authors declare that they have no other competing interests. **Data and materials availability:** All data needed to evaluate the conclusions in the paper are present in the paper and/or the Supplementary Materials.

Submitted 25 June 2024
Accepted 12 December 2024
Published 15 January 2025
10.1126/sciadv.abm9843